

The EFIGI catalogue of 4458 nearby galaxies with detailed morphology

A. Baillard^{1,2}, E. Bertin^{1,2}, V. de Lapparent^{1,2}, P. Fouqué^{3,4}, S. Arnouts^{5,6,7}, Y. Mellier^{1,2}, R. Pelló^{3,4}, J.-F. Leborgne^{3,4}, P. Prugniel^{8,9,10}, D. Makarov^{8,9,10,11}, L. Makarova^{8,9,10,11}, H.J. McCracken^{1,2}, A. Bijaoui^{12,13}, and L. Tasca^{5,6}

¹ Université Pierre et Marie Curie-Paris 6, Institut d'Astrophysique de Paris, 98 bis Boulevard Arago, F-75014 Paris, France

² CNRS, UMR 7095, Institut d'Astrophysique de Paris, 98 bis Boulevard Arago, F-75014 Paris, France

³ Université Paul Sabatier-Toulouse III, Laboratoire d'Astrophysique de Toulouse Tarbes, 14 Avenue Edouard Belin, F-31400 Toulouse, France

⁴ CNRS UMR 5572, Laboratoire d'Astrophysique de Toulouse Tarbes, 14 Avenue Edouard Belin, F-31400 Toulouse, France

⁵ Université de Provence Aix-Marseille 1, Laboratoire d'Astrophysique de Marseille, Traverse du Siphon-Les trois Lucs, BP 8, F-13376 Marseille Cedex 12, France

⁶ CNRS UMR 6110, Laboratoire d'Astrophysique de Marseille, Traverse du Siphon-Les trois Lucs, BP 8, F-13376 Marseille Cedex 12, France

⁷ Canada-France-Hawaii Telescope Corporation, Kamuela, HI-96743, USA

⁸ Université Claude Bernard Lyon 1, Centre de Recherche Astronomique de Lyon, Observatoire de Lyon, St. Genis Laval, F-69561, France

⁹ CNRS UMR 5574, Centre de Recherche Astronomique de Lyon, Observatoire de Lyon, St. Genis Laval, F-69561, France

¹⁰ ENS-L, Ecole Normale Supérieure de Lyon, Centre de Recherche Astronomique de Lyon, Observatoire de Lyon, St. Genis Laval, F-69561, France

¹¹ Special Astrophysical Observatory, Nizhnij Arkhyz, Zelenchukskij region, Karachai-Cirkassian Republic, Russia 369167

¹² Université de Nice Sophia-Antipolis, Observatoire de la Côte d'Azur, BP 4229, F-06304 Nice Cedex 4, France

¹³ CNRS UMR 6202, Observatoire de la Côte d'Azur, BP 4229, F-06304 Nice Cedex 4, France

Received December 31, 2010; accepted March 22, 2011

ABSTRACT

Context. Now that modern imaging surveys have produced large databases of galaxy images advanced morphological studies have become possible. This has driven the need for well-defined calibration samples.

Aims. We present the EFIGI catalogue, a multi-wavelength database specifically designed to densely sample all Hubble types. The catalogue merges data from standard surveys and catalogues (Principal Galaxy Catalogue, Sloan Digital Sky Survey, Value-Added Galaxy Catalogue, HyperLeda, and the NASA Extragalactic Database) and provides detailed morphological information.

Methods. Imaging data were obtained from the SDSS DR4 in the u , g , r , i , and z bands for a sample of 4458 PGC galaxies, whereas photometric and spectroscopic data were obtained from the SDSS DR5 catalogue. Point-spread function models were derived in all five bands. Composite colour images of all objects were visually examined by a group of astronomers, and galaxies were assigned positions in the Hubble sequence and classified according to 16 morphological attributes describing their structure, texture, environment and appearance on a five-level scale.

Results. The EFIGI Hubble sequence is in remarkably good agreement with the RC3 Revised Hubble Sequence. The main characteristics and reliability of the catalogue are examined, including photometric completeness, type mix, systematic trends and correlations.

Conclusions. The final EFIGI database is a large sub-sample of the local Universe which densely samples Sd, Sdm, Sm and Im types compared to magnitude-limited catalogues. We estimate that the photometric catalogue is more than $\approx 80\%$ complete for galaxies with $10 < g < 14$. More than 99.5% of EFIGI galaxies have known redshifts in the HyperLeda and NED databases.

Key words. Astronomical data bases - Astronomical databases: miscellaneous - Catalogs - Surveys - Galaxies: fundamental parameters - Galaxies: elliptical and lenticular, cD - Galaxies: spiral - Galaxies: dwarf - Galaxies: peculiar - Galaxies: interactions - Galaxies: bulges - Galaxies: clusters: general - Galaxies: groups: general - Galaxies: luminosity function, mass function - Galaxies: statistics - Galaxies: photometry - Galaxies: star formation - Galaxies: structure

1. Introduction

The morphological analysis of galaxies is a problem of interest in astronomy because it provides us with important clues concerning the evolutionary processes of these objects (Gray et al. 2009). Morphology is strongly correlated with physical properties (Bertin & Lin 1996; Colpi et al. 2006; Seigar et al. 2008) and morphological classification is often considered as a convenient way to distinguish between galaxies that have different physical properties (see Buta 2011, for a recent review). The first widely

used system was Hubble's "tuning fork" (Hubble 1936), where galaxies are assigned a visual classification (elliptical, lenticular, spiral or irregular). Among other improvements, the revised Hubble system (RHS, de Vaucouleurs 1959) added a numerical "stage" $-6 \leq T \leq +10$ which allows intermediate states to be considered.

Apart from the issue of classification schemes, many properties of galaxies have been explored to describe morphology. The bulge-to-disk ratio (de Jong et al. 2005) and the degree of azimuthal variation of surface brightness are often used as discrim-

inant parameters along the Hubble sequence. Other features such as rings, dust, or colour are also useful for understanding how galaxies evolve (Buta & Combes 1996). Some analyses based on particular features (e.g. Naim et al. 1996, Buta et al. 2006) have shown that the Hubble type is not sufficient for describing all galaxy properties. Complementary descriptors of galaxy shapes are particularly important at redshifts ≥ 1 , where a higher fraction of objects appear highly distorted and cannot be easily classified according to the Hubble scheme in place at lower redshifts (Abraham et al. 2003).

The volume of well-resolved galaxy images provided by modern imaging surveys such as the Sloan Digital Sky Survey (SDSS) or the CFHTLS¹ (Canada-France-Hawaii Telescope Legacy Survey) is too large to be analysed by eye by individual astronomers, and must be carried out by automatic software tools or through *crowdsourcing* initiatives like the “Galaxy Zoo” project (Lintott et al. 2008). Whether crowdsourcing or automatic morphometry techniques are used, a well-defined calibration set is essential.

This paper describes the EFIGI catalogue, a catalogue of 4458 galaxies with digital images and detailed morphological information. The aim of the EFIGI² (“Extraction de Formes Idéalisées de Galaxies en Imagerie”) project is to build automated morphometry measurement and classification systems operating on resolved galaxy images. The direct motivation for creating the EFIGI catalogue is the need for suitable morphological data to train supervised learning machines. The EFIGI morphological description therefore includes the Hubble Type and 16 attributes estimated by eye, which are specifically designed to describe the various components of a galaxy: bulge, arms and other dynamical features (bars, rings); textures (dust, flocculence, hotspots, etc.); inclination along the line of sight; and environment (contamination, multiplicity). We also provide FITS images, Point-Spread Function (hereafter PSF) estimates, and spectroscopic data extracted from existing catalogues.

This paper is organised as follows: Section 2 introduces the data, the catalogues used as a reference and the whole compilation process. In Section 3, we describe in detail the morphological sequence and the various attributes and check for the absence of obvious trends in the final sample, and study correlations among attributes. Section 4 presents the PSF estimates obtained with our software. Section 5 gives an overview of the properties of the resulting catalogue in terms of sky coverage, clustering, photometric completeness, morphological fractions and redshift distribution. Finally, Section 6 compares the EFIGI catalogue with the recent morphological catalogue by Nair & Abraham (2010). A summary and an prospects for future uses are finally addressed in Section 7.

2. Data and selection process

Data are extracted from the Third Reference Catalogue of Bright Galaxies (RC3), the Principal Galaxy Catalogue (PGC), the Sloan Digital Sky Survey (SDSS), the New York University Value-Added Galaxy Catalogue (NYU-VAGC), HyperLeda, and the NASA Extragalactic Database (NED).

2.1. Master list

The master list of EFIGI catalogue galaxies is a subset of the Third Reference Catalogue of Bright Galaxies (RC3, de

Vaucouleurs et al. 1991). We extract from the RC3 15 columns (see Table A.3), including the sky coordinates, position angle, R_{25} aspect ratio, D_{25} diameter³, Hubble type T , and the associated error e_T . Galaxies are designated by their PGC (Paturel et al. 1995) number. Since 1995, the RC3 has been enlarged but neither renamed nor revised. Consequently, it is reasonably complete for galaxies with an apparent diameter larger than 1 arcmin at the $\mu_B = 25$ mag.arcsec⁻² isophotal level, a total B-band magnitude (B_T) brighter than about 15.5, and a recession velocity lower than 15,000 km s⁻¹ (Paturel et al. 2003). In addition to objects already listed in the RC2 (de Vaucouleurs et al. 1976), the RC3 includes objects of special interest, such as compact galaxies smaller than 1 arcmin or fainter than magnitude 15.5. The number of RC3 objects meeting both diameter and magnitude conditions is 11,897. Adding objects meeting only the diameter or the magnitude criterion, and objects of interest smaller than 1 arcmin, fainter than 15.5, or with a velocity $> 15,000$ km s⁻¹, brings the total number of galaxies to 23,011.

A column of particular interest in this work is the error estimate on the Hubble type (e_T), which, when present, indicates that a galaxy has been classified by several astronomers. To ensure that the Hubble stages T indicated in our master list are sufficiently reliable, the EFIGI catalogue contains only RC3 objects with known e_T , or with a Hubble type 90 (non-Magellanic irregulars).

2.2. Imaging data

The fourth release of the SDSS (DR4, Adelman-McCarthy et al. 2006) provides the imaging material for the EFIGI database. The SDSS DR4 offers *ugriz* CCD imaging for about 6851 deg² of the Northern Galactic sky complemented with spectroscopy for galaxies with $r < 17.77$ magnitude over 4681 deg². The EFIGI catalogue contains only galaxies for which there is imaging in all 5 bands in the SDSS DR4.

For each galaxy, up to nine DR4 survey (“fpC”) frames closest to the coordinates are obtained directly from the SDSS DAS server⁴ in all five u , g , r , i and z bands. The original catalogue coordinates often appear to be too imprecise for unambiguous identification, hence for each PGC galaxy satisfying the criteria listed in Sect. 2.1, better J2000 coordinates are obtained through the CDS Sesame name resolver service (Bonnarel et al. 2000; Schaaff 2004). We corrected the coordinates of 47 galaxies that appear to be off by more than ~ 10 arcseconds, based on the SDSS images (the corrected coordinates are listed in Table A.2). Finally, we exclude a few objects, for which no non-ambiguous match can be made, and we only keep one galaxy in pairs of identical objects with a different PGC name.

Each set of fpC images is automatically background-subtracted, rescaled, and combined using the SWARP software (Bertin et al. 2002). SDSS images are properly sampled, which allows us to use a Lanczos3 interpolant to minimise resampling artifacts. Two sets of data are produced at this stage: the first data set is meant for visual inspection; the second one, with a slightly larger field of view, contains the actual EFIGI science images released in FITS format. For the “visual” dataset, galaxy images are scaled and framed to 255x255 pixels in such a way that the RC3 blue isophote at $\mu = 25$ mag arcsec⁻² fits exactly onto the central area of 169x169 pixels. This is done by setting the output pixel scale to $9 \times \text{dexp}(\log D_{25})/256$ arcsec, where $\log D_{25}$ is taken from the RC3 catalogue. Science dataset images have the

¹ <http://cfht.hawaii.edu/Science/CFHTLS/>

² <http://www.efigi.org>

³ The description of all catalogue fields is given in Appendix A.

⁴ <http://das.sdss.org>

same number of pixels, but the angular pixel scale is 33% larger pixel on each axis. We do not apply any flux correction after rescaling, as our goal is to build a collection of galaxy images with a constant zero-point in apparent surface brightness in each band. We check all images by eye, and discard from the sample all galaxies for which at least one of the visual dataset images is completely ruined by artifacts or missing data, ending up with a final EFIGI selection of 4458 galaxies. Galaxy images partly contaminated by bright stars or satellite trails are intentionally kept to provide a realistic sampling of survey conditions.

Finally, all *i*, *r*, and *g* frames are used to make composite “true colour” RGB images in PNG format with the STIFF software⁵, using the same intensity mapping parameters for all RGB images. In order to provide an optimal rendering of objects under typical screen viewing conditions, a gamma correction of 1.3 is applied to the luminance component (supplementing the regular RGB gamma of 2.2), and colour saturation is exaggerated by a factor 2.0.

2.3. SDSS photometric and spectroscopic cross-identifications

Identifying EFIGI galaxies in the SDSS catalogue allows us to find a unique identifier necessary to unambiguously extract both photometric and spectroscopic data from any existing or future release of the SDSS catalogues. Although the EFIGI imaging data come from SDSS DR4, SDSS photometric and spectroscopic catalogue data are extracted from the DR5.

At the start of the project, we matched the positions of the objects by querying the SDSS DR5 database⁶ for all objects within a radius of 0.1 arcmin from the list of 4458 corrected coordinates. 3942 objects IDs were found in the DR5 photometric data. To complete the set, a manual match was made using the SDSS DR5 finding tool and 423 additional objects are found. The automatic search often fails because of deblending problems which results in the galactic nucleus being classified as a star. The SDSS detection is sometimes located far from the galaxy barycentre and tens of other objects (real or false sources) are closer and thus detected first. In the end, 93 objects were left without DR5 photometric data. We used the corrected coordinates of these objects to locate them within the DR7 using the “Navigate” SDSS visual tool⁷ which allowed us to find additional photometric identifications for 37 galaxies. The remaining 56 galaxies without SDSS photometric data are all sources located outside the sky region scanned by the SDSS pipeline.

The SDSS photometric identifications allow one to retrieve the airmasses, zero points (*aa*) and extinction coefficients (*kk*), which are necessary to correct flux measurements. We also use the unique SDSS object ID to perform SQL queries on the SDSS DR7 *SpecObj* table; this yields 3136 EFIGI galaxies with spectroscopic data from the SDSS DR7. The SDSS retrieved fields are listed in Table A.6.

2.4. VAGC

The NYU-VAGC (Blanton et al. 2005) is a cross-matched collection of galaxy catalogues extracted from the SDSS, which includes carefully constructed large-scale galaxy structure samples. We use the version based on the SDSS DR4. The most useful component of the catalogue for our purposes is the low-

redshift sample ($10 < d < 150 \text{ Mpc h}^{-1}$), which provides redshifts corrected for the Local Group motion, and k-corrections in all SDSS *ugriz* bands (Blanton & Roweis 2007). Because the VAGC is extracted from the SDSS, objects can easily be cross-identified in both catalogues using *plate*, *fiberID* and *MJD* fields.

2.5. HyperLeda

HyperLeda (Paturel et al. 2003) is a merging of several catalogues, and is originally based on the PGC. It also provides morphological data (bar, ring and compactness). Cross-identification with HyperLeda is simply done using the PGC number. All EFIGI objects are found. The columns retrieved from HyperLeda are listed in Table A.4. Particularly useful are velocities corrected for the Virgocentric infall of the Local Group. All other names for the PGC objects are also extracted from HyperLeda, in which 50 different catalogues are referenced.

2.6. NED

NED is a database obtained by merging data from many sources. Its most appealing features for the EFIGI catalogue are redshift measurements and cluster searches (see Sect. 5.2). Searching NED using PGC names yields a total of 4404 objects with known redshifts (see Table A.5).

2.7. EFIGI catalogue

To summarise, the EFIGI catalogue is composed of 4458 galaxies with:

- PGC data
- SDSS images in 5 bands and object identifiers
- HyperLeda data
- NED data
- VAGC data (incomplete)

Among these objects:

- 4402 have SDSS DR7 photometric catalogue data
- 3136 have SDSS DR7 spectroscopic catalogue data
- 4415 have redshifts from HyperLeda
- 4404 have redshifts from NED
- 1729 have NYU-VAGC low-z data

Comparison of the redshifts of each object among the different catalogues allows us to find some rare erroneous redshifts in the HyperLeda, NED et SDSS catalogues (see de Lapparent et al. 2011).

3. The EFIGI morphological description

3.1. Morphological sequence

The EFIGI morphological classification is defined by slightly modifying the RC3 Hubble classification: the main galaxy sequence is identical to that of the RC3, but peculiar galaxies and special features are no longer considered as separate stages. The resulting classification, which we call the EFIGI Hubble Sequence (EHS) is summarised in Table 1.

There are many similarities between the RC3 and the EHS. Compact elliptical galaxies are rare and difficult to distinguish, and cD galaxies exhibit a more peaky light profile with more

⁵ <http://astromatic.net/software/stiff>

⁶ <http://cas.sdss.org/astrodr5/en/tools/search/IQS.asp>

⁷ <http://cas.sdss.org/astrodr7/en/tools/chart/navi.asp>

Table 1. The EFIGI Hubble Sequence (EHS). The left column lists the class (elliptical, lenticular, spiral, irregular, Dwarf) and the second column the intermediate stage within each class. The third and fourth columns give respectively the literal type and the EHS code for each corresponding EFIGI type. The last column briefly describes the class.

Class	Stage	Literal type	EHS type	Description
Ellipticals				Ellipse or sphere. Structureless, smooth intensity distribution with relatively steep gradient.
Elliptical	Compact	cE	-6	Compact elliptical.
Elliptical	0-6	E	-5	More or less elongated.
Elliptical	cD	cD	-4	Giant elliptical. Sharp central profile and very extended low surface brightness halo.
Lenticulars				Spheroidal bulge and disk but no visible spiral arms in the disk.
Lenticular	Early	S0 ⁻	-3	Dominant bulge, no sign of structure in disk nor dust.
Lenticular	Intermediate	S0 ⁰	-2	Some structure in disk but no arms, low amounts of dust.
Lenticular	Late	S0 ⁺	-1	Clear structure in disk but no arms, thin dust lanes.
Spirals				Central bulge and disk with spiral arms. May harbour a bar.
Spiral	0/a	S0/a	0	Very tightly wound arms, very prominent bulge, low amounts of dust
Spiral	a	Sa	1	Tightly wound arms, very prominent bulge, low amounts of dust
Spiral	ab	Sab	2	Quite tightly wound arms, prominent bulge, low amounts of dust
Spiral	b	Sb	3	Quite tightly wound arms, prominent bulge, strong dust lanes
Spiral	bc	Sbc	4	Quite loosely wound arms, medium bulge, dust lanes
Spiral	c	Sc	5	Grand design spiral, fairly weak bulge, dust lanes
Spiral	cd	Scd	6	Loosely wound and weak arms, weak bulge, scattered dust
Spiral	d	Sd	7	Loosely wound and very weak arms, weak bulge, scattered dust
Spiral	dm	Sdm	8	Very loosely wound arms, very weak bulge, low amounts of dust
Spiral	m	Sm	9	Some indication of spiral arms, very weak bulge, low amounts of dust
Irregular	Magellanic	Im	10	No arms, no bulge. Irregular profile. Low surface brightness. May host a bar.
Dwarf	Dwarf spheroidal elliptical	dE	11	Regular low surface brightness profile, no arms. May contain a tight nucleus.

diffuse wings than common elliptical galaxies. Lenticular galaxies usually look more elongated than elliptical galaxies and their Bulge/Total flux ratio (B/T hereafter) decreases going from S0⁻ to S0⁺. Among spiral galaxies, Sa types have the highest B/T whereas Sm have no bulge. Also, Sa arms are the most tightly wound and Sm arms are the most open. The major distinction between Sm and Im galaxies is that the former have indications of a spiral arm pattern that is not visible in the latter.

Table 1 shows that the one difference between the RC3 and EHS is that the RC3 elliptical galaxy stages 0 to 6, indicating the elongation of the elliptical galaxy, are not specified in the EHS. Other differences are for irregular and dwarf elliptical galaxies. Whereas the RC3 Magellanic irregular type matches the Im type in the EFIGI classification sequence, the RC3 includes the additional class of non-Magellanic irregular galaxies (type 90, literal type I0) that is not used in the EHS. These objects are considered as a “perturbed” version of some “regular” stage, whose amount of perturbation is measured by the perturbation attribute (see next sub-section).

Moreover, in contrast to the RC3, the EFIGI dwarf elliptical galaxies are kept in a separate class from ellipticals. Dwarf ellipticals have smooth elliptical isophotes reminiscent of early type galaxies but their bluer colours, lower surface brightness and closer to exponential profiles are more typical of later type galaxies (Ferguson & Binggeli 1994; Kormendy et al. 2009a); many of these galaxies are also nucleated (Binggeli & Cameron 1991). This class also includes dwarf lenticular galaxies (dS0), with indications of a lens or a bar feature (Sandage & Binggeli 1984; Binggeli & Cameron 1991). We also include in the dE class dwarf spheroidal galaxies (dSph), the lowest luminosity galaxies known, and which have a flatter surface brightness profile than dE galaxies, and less regular shapes. Kormendy et al. (2009b) also merge all these objects into the single class of “Spheroidal” galaxies.

Finally, galaxies that have some abnormality in shape, size, or content which sets them apart from the normal ellipticals, spirals, irregulars and dwarf ellipticals are said to be “peculiar” in the RHS. Peculiar galaxies often result from galaxy interactions or galaxy mergers, and thus may have distorted isophotes. They may also show some other distinctive feature such as jets emerging from the nucleus, or unusual amounts of dust. In the RHS, they are denoted by the addition of “p” or “pec” to their main classification type and are classified separately (type 99). In the EFIGI classification, peculiarity is described by a set of attributes (see next sub-section) rather than by stage.

3.2. Attribute definition

Attributes are defined primarily according to their ability to characterise the morphology of galaxies and their relevance to the physical properties of the objects. Attribute measurements (morphometry) must nevertheless be able to describe the morphological properties of the known types along the Hubble sequence and any deviation from those types (Roberts & Haynes 1994; Baillard 2008).

The EFIGI attributes can be divided into six groups:

- Appearance: inclination/elongation
- Environment: multiplicity, contamination
- Bulge: B/T ratio
- Spiral arm properties: arm strength, arm curvature, rotation
- Textural aspect: visible dust, dust dispersion, flocculence, hot spots
- Dynamical features: bar length, inner ring, outer ring, pseudo-ring, perturbation

Most attributes are not binary (for instance inclination/elongation, B/T or dust dispersion),

hence it is important to set a scale describing their strength. We choose a scale with five steps (0 to 1, by steps of 0.25), which provides two intermediate values between the median and each of the extreme values; a higher number of steps would have been irrelevant and confusing in a context of visual identification.

In order to facilitate comparison with automatic techniques, we decided to make attribute strength a monotonically increasing function of the fraction of flux held in each feature relative to that of the whole galaxy, whenever applicable (contamination, arm strength, hot spots, inner ring, outer ring, pseudo-ring); it is also evidently the case for B/T. Flux fractions are visually estimated from the composite *irg* 3-colour image, and the function may not be linear. For attributes B/T, inclination/elongation, multiplicity, and rotation, the strength scale ranges between the extreme possible values. For all other attributes, the strength scale ranges between the most extreme cases found in the EFIGI catalogue.

For each attribute of each galaxy, a 70% confidence interval is also estimated by setting a lower and upper limit among the five possible attribute values of 0, 0.25, 0.5, 0.75 and 1.0. The narrowest possible confidence interval is 0.25, the widest is 1.0. When an attribute is not defined for a given galaxy, it is set to 0.5 with lower and upper confidence limits at 0 and 1 respectively.

3.2.1. Inclination/elongation

For galaxies with a visible disk (lenticulars and spirals), this attribute measures the disk inclination $f = 1 - \cos\theta$, where θ is the angle between the rotation axis of the disk and the line-of-sight of the observer, or equivalently between the galaxy disk and the plane of the sky; θ then varies from 0° (face-on) to 90° (edge-on). For galaxies with no evident disk (ellipticals, cD, cE, Im and dE), this attribute provides an estimate of the apparent elongation of the object, that is $f = 1 - b/a$ with a and b the apparent major and minor axes lengths respectively. The scale of elongation is matched to that of inclination so that a circular disk of a given inclination attribute value would have an identical elongation attribute value. Values of the attribute are:

0	0° - 35° disk inclination angle (face-on) or very low elongation $f < 0.2$
0.25	35° - 50° disk inclination angle or low elongation $0.2 < f < 0.4$
0.5	50° - 70° disk inclination angle or moderate elongation $0.4 < f < 0.7$
0.75	70° - 80° disk inclination angle or strong elongation $0.7 < f < 0.8$
1	80° - 90° disk inclination angle (edge-on) or very strong elongation $f > 0.8$

3.2.2. Multiplicity

This attribute quantifies the abundance of galaxies in the vicinity of the main galaxy. Only galaxies that have magnitudes less than that of the main galaxy plus ~ 5 mag, and whose centre lies within $0.75 D_{25}$ from the image centre are counted. Values are:

0	no other galaxy
0.25	one neighbouring galaxy
0.5	two neighbouring galaxies
0.75	three neighbouring galaxies
1	four or more neighbouring galaxies

3.2.3. Contamination

This attribute indicates the severity of the contamination by bright stars, overlapping galaxies or image artifacts (diffraction spikes, star halos, satellite trails, electronic defects). Values are:

0	no overlapping source visible on the galaxy isophotal footprint
0.25	only faint sources overlapping the galaxy isophotal footprint (negligible effect on photometry and morphometry)
0.5	overlapping sources on the galaxy isophotal footprint or faint gradient/background light pollution (some impact on photometry and morphometry)
0.75	bright sources overlapping the galaxy isophotal footprint or strong gradient/background light pollution (large impact on photometry and morphometry)
1	most of the galaxy image footprint dominated by light from a very bright contaminant (unreliable photometry or morphometry).

3.2.4. Perturbation

This attribute measures the amplitude of distortions in the galaxy profile, due to tidal effects for instance. 0 indicates a light profile with rotational symmetry (hence regular spiral arms when applicable), while 1 corresponds to the most distorted galaxies observed in the catalogue. Values are:

0	No distortion
0.25	Slight distortion of the object profile and/or the spiral arms
0.5	Moderate distortion of the object profile and/or the spiral arms
0.75	Strong distortion of the object profile, with profile components (bulge, disk, spiral arms) still identifiable
1	Completely distorted profile, components can be barely distinguished

3.2.5. Bulge/Total ratio

This attribute measures the relative contribution of the bulge (spheroidal) component to the total flux of the galaxy. For instance, Im galaxies have $B/T = 0$ and elliptical galaxies have $B/T = 1$. Values are:

0	no bulge
0.25	very weak bulge comprising $\sim 25\%$ of the total flux
0.5	medium bulge comprising $\sim 50\%$ of the total flux
0.75	strong bulge comprising $\sim 75\%$ of the total flux
1	all flux within bulge, no disk nor spiral arms

3.2.6. Arm strength

This attribute measures the relative strength of spiral arms, in terms of the flux fraction relative to the whole galaxy. 0 indicates no visible arms, while 1 corresponds to the highest fraction observed in the EFIGI sample. When no spiral arms are visible (either due to the galaxy structure or to a high inclination that prevents any existing arm to be seen), this attribute is undefined. Defined values are:

0	Very weak or no spiral arms
0.25	weak contribution of the spiral arms to the galaxy flux
0.5	moderate contribution of the spiral arms to the galaxy flux
0.75	significant contribution of the spiral arms to the galaxy flux
1	highest contribution of the spiral arms to the galaxy flux

3.2.7. Arm curvature

This attribute measures the average intrinsic curvature of the spiral arms, that is for the same galaxy seen face-on, as inclination increases the variations of the arm curvature along the arms. It is subordinate to the `arm strength` attribute: for all EFIGI galaxies for which `arm strength` is undefined, and for the majority of EFIGI galaxies with `arm strength` equal to 0, specifically those with no visible spiral arms, `arm curvature` has no meaning and the attribute is undefined. Defined values are:

0	wide open spiral arms, with pitch angles of 40 degrees or more
0.25	open spiral arms, with pitch angles of 30 to 40 degrees
0.5	moderately open spiral arms, with pitch angles of 20 to 30 degrees
0.75	closed-in spiral arms, with pitch angles of 10 to 20 degrees
1	tightly wound spiral arms, with pitch angles of 10 degrees or less

3.2.8. Rotation

This attribute indicates whether the spiral pattern appears to rotate clockwise (East of North negative) or counterclockwise (East of North positive). It is subordinate to the `arm strength` attribute: for the vast majority of EFIGI galaxies with `arm strength` equal to 0, specifically those with no visible spiral arms, `rotation` has no meaning and the attribute is undefined. Defined values are:

0	definitely clockwise
0.25	probably clockwise
0.5	no preferred direction
0.75	probably counterclockwise
1	definitely counterclockwise

3.2.9. Visible dust

This attribute measures the strength of features revealing the presence of dust: obscuration and/or diffusion of star light by a dust lane or molecular clouds. Values are:

0	no dust
0.25	indications of dust, but dust cannot be located
0.5	low to moderate amounts of dust, can be located
0.75	significant amounts of dust covering < 50% of the surface of the galaxy
1	high amounts of dust covering > 50% of the surface of the galaxy

3.2.10. Dust dispersion

This attribute measures the “patchiness” of the dust distribution in terms of whether the dust is smoothly distributed in sharp lanes (or rings) or distributed in strongly irregular patches. This

attribute is subordinate to the `visible dust` attribute : `dust dispersion` is undefined when `visible dust` is equal to 0 or 1. Defined values are:

0	Thin lane(s) of dust with smooth outline
0.25	Thin lane(s) of dust with patchy outline
0.5	Patchy lane(s) of dust and some other small patches
0.75	Very patchy lane(s) of dust and many other patches
1	Extremely patchy distribution of the dust

3.2.11. Flocculence

This attribute measures the importance of “flocculent” features due to scattered HII regions relative to the strength of spiral arms and the underlying smooth profile components. Values are:

0	no visible flocculence
0.25	weak/barely visible flocculence/patchiness limited to small parts of the galaxy disk
0.5	some flocculence visible in parts of the galaxy disk
0.75	significant flocculence over most of the galaxy disk
1	strong flocculence over most of the galaxy disk

3.2.12. Hot spots

This attribute indicates the presence of “hot spots”, that is regions with a very high surface brightness such as giant regions of star formation, active nuclei, or stellar nuclei of dwarf galaxies. It is not to be confused with scattered HII regions of normal intensity contributing to the “flocculent” aspect of some disks. Values are:

0	no hot spot
0.25	small part of the galaxy flux included in one or several hot spots
0.5	moderate part of the galaxy flux included in one or several hot spots
0.75	significant part of the galaxy flux included in one or several hot spots
1	one or several hot spots dominate the galaxy flux

3.2.13. Bar length

This attribute quantifies the presence of a central bar component in the galaxy. Contrary to other attributes, the flux fraction may not be the most physically-relevant quantifier for bar strength. Another possible quantifier is bar elongation which is found to correlate strongly with bar torque in some samples (Block et al. 2001; Laurikainen et al. 2002). Unfortunately, elongation cannot always be estimated reliably on ground-based images, especially for short bars which can be very thin. Bar length (relative to the galaxy D_{25}) is a more convenient quantifier, and has been chosen here as the criterion to quantify bar strength. This attribute is often undefined for highly inclined disks in which one cannot assess the presence of a bar. Defined values are:

0	no visible bar
0.25	short, barely visible bar feature
0.5	short bar, with a length about one third of D_{25}
0.75	long bar, that extends over about half of D_{25}
1	very long, prominent bar that extends over more than half of D_{25}

3.2.14. Inner ring

This attribute measures the presence of a circular or elliptical ring-like overdensity that is within the disk and/or spiral arm

pattern, and at the end of the bar when present (contrary to nuclear rings that occur well within the bar). This attribute also includes inner lenses, that is regions of nearly constant surface brightness with radius, as well as the inner pseudo-rings, which are not completely closed and more spiral-like. Strength is proportional to the fraction of galaxy light contained within the ring. A value of 1 corresponds to the highest fraction observed in the catalogue. This attribute is undefined for highly inclined disks in which one cannot assess the presence of a ring. Defined values are:

- 0 no inner ring
- 0.25 low ring contribution to the galaxy flux
- 0.5 intermediate ring contribution to the galaxy flux
- 0.75 significant ring contribution to the galaxy flux
- 1 highest ring contribution to the galaxy flux

3.2.15. Outer ring

This attribute measures the presence of a circular or elliptical ring-like over-density that lies mostly outside the disk and/or spiral arm pattern. This attribute also includes outer lenses, that is regions of nearly constant surface brightness with radius. Strength is proportional to the fraction of galaxy light contained within the ring. A value of 1 corresponds to the highest fraction observed in the catalogue. This attribute is undefined for highly inclined disks in which one cannot assess the presence of a ring. Defined values are:

- 0 no outer ring
- 0.25 low ring contribution to the galaxy flux
- 0.5 intermediate ring contribution to the galaxy flux
- 0.75 significant ring contribution to the galaxy flux
- 1 highest ring contribution to the galaxy flux

3.2.16. Pseudo-Ring

This attribute measures the presence of outer pseudo-rings as defined by Buta & Combes (1996): the R'_1 ring, having a dimpled “eight” shape due to a 180° winding of the spiral arms with respect to the end of a bar; the R'_2 feature, with a higher winding of 270° of the spiral arms with respect to the bar; and the intermediate $R_1R'_2$ pattern.

Values of 0.75 and 1 are assigned to galaxies having two closed-loop arms of type R'_1 , and grades the fraction of the total galaxy light that is included in the pseudo-ring feature. Values of 0.25 and 0.5 are attributed to galaxies for which one or both of the arms do not form a closed-loop of type R'_1 , thus including types R'_2 and $R_1R'_2$ from Buta & Combes (1996), and also grade the fraction of the total galaxy light that is included in the pseudo-ring feature. This attribute is undefined for highly inclined disks in which one cannot assess the presence of a pseudo-ring. Defined values are:

- 0 no visible pseudo-ring feature
- 0.25 R'_2 and $R_1R'_2$ pseudo-rings containing a low fraction of the galaxy flux
- 0.5 R'_2 and $R_1R'_2$ pseudo-rings containing a higher fraction of the galaxy flux
- 0.75 R'_1 pseudo-ring feature containing a low fraction of the galaxy flux
- 1 R'_1 pseudo-ring feature containing a higher fraction of the galaxy flux

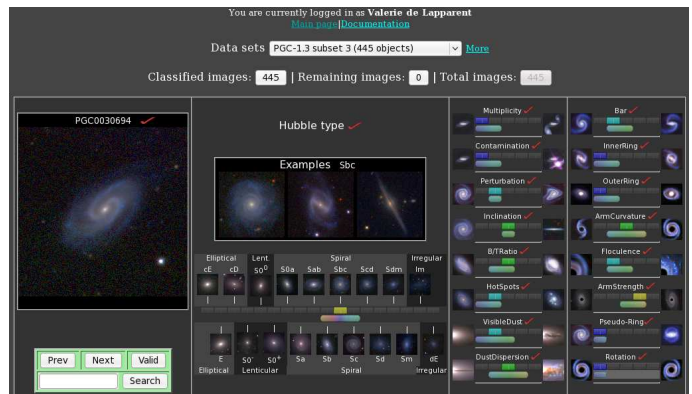


Fig. 1. Screenshot of *Manclass*, the classification interface. The galaxy to be classified is shown on the left. The EHS sliders and three prototypes (face-on, edge-on and barred) are displayed in the middle. The attribute sliders are located in the rightmost portion of the frame.

3.3. Classification process

In order to test the EFIGI morphological classification and attribute definition, a common set of 100 galaxies is extracted from the whole sample and classified by 11 astronomers among the authors of this article (S. Arnouts, A. Baillard, E. Bertin, P. Fouqué, V. de Lapparent, J.-F. Le Borgne, D. Makarov, L. Makarova, H.J. McCracken, Y. Mellier, R. Pelló). Statistics are automatically computed for each astronomer measuring his/her mean confidence, and comparing his/her classification with those of the other astronomers and with the RC3 morphological type. This step allows each astronomer to estimate his/her relative biases and adjust his/her classification with that of others. Classifying this small sample also allows the astronomers to adjust the final EHS. Then the full sample is divided into 10 sub-samples of 445 galaxies which are all, with one exception, classified by one astronomer (one sample is classified by several astronomers).

An interactive interface called “Manclass” has been designed to ease the visual classification process. A snapshot is shown Fig. 1. This interface displays for each galaxy the *irg* colour image, and 17 double sliders corresponding to the EHS and the 16 EFIGI attributes. The interface allows the astronomer to define for all examined galaxies a triplet of values for each attribute: the mode, defined as the value considered to be the closest to the correct stage or attribute strength, and the two boundaries of the 70% confidence interval (see Sect. 3.2), which is not necessarily centred on the mode. This is particularly useful for defining a plausible EHS interval. For both the EHS and the attributes, the upper slider adjusts the mode and the lower bar sets the confidence interval.

Using the *irg* “true colour” images created from the SDSS imaging data, a subset of 3 images has been selected as reference for each EHS stage: a face-on non barred galaxy, a face-on barred galaxy, and an edge-on galaxy. These are shown when the mouse slides across the EHS slider, and the face-on non barred galaxy image is shown as a fixed “thumbnail” next to each position of the EHS slider. Moreover, 2 “true colour” comparison images have been selected as templates for each extreme strength values of the attributes and are displayed as “thumbnails” at the limit of each corresponding slider.

Once the 4458 galaxies have been classified, a long process of visual homogenisation of attribute strengths takes place. Contrary to the classification of the sub-samples of 445 galaxies by each astronomer, homogenisation is performed sepa-

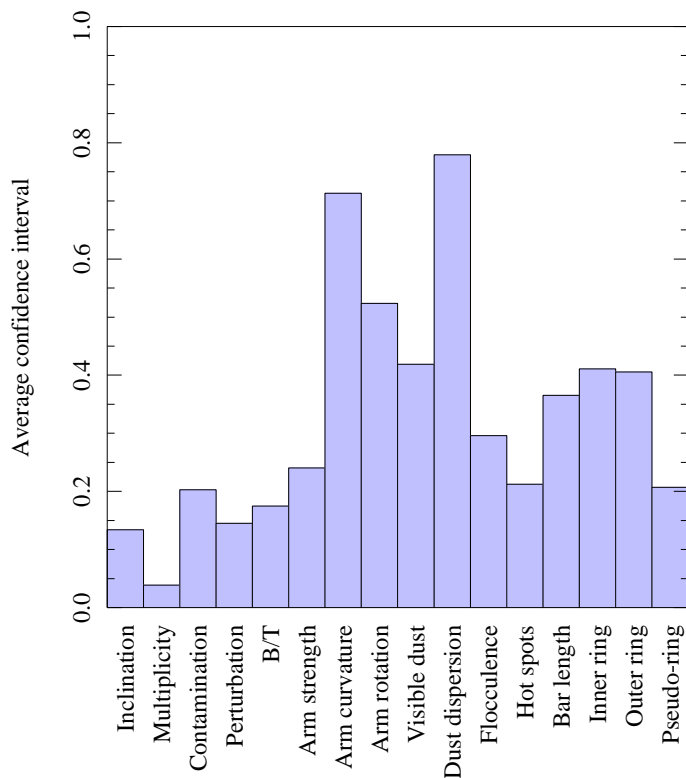


Fig. 2. Average confidence intervals of EFIGI attributes in the homogenised data set (only confidence intervals < 1 are considered).

rately for each attribute, and by two astronomers: E. Bertin for multiplicity, contamination, B/T ratio, bar length, hot spots, flocculence, rotation and V. de Lapparent for perturbation, inclination/elongation, visible dust, dust dispersion, internal ring, external ring, eight shape, arm strength, arm curvature and the EHS. A variant of the “Manclass” interface is used for the homogenisation, which displays mosaics of galaxy images, together with the slider of the attribute under consideration below each image. Homogenisation is particularly useful for attributes that are difficult to estimate. Arm Curvature and Dust dispersion have the widest confidence intervals in Fig. 2 and were the most difficult to grade, contrary to Multiplicity and Inclination, which have the lowest error estimates.

The homogenisation process requires several passes through the data in order to first define for each attribute a well-defined scale, then to train the observer’s eye in order to have a stable classification, and finally to check for biases and spurious correlations with other attributes. Inter-user statistics are used to derive useful hints about attributes and astronomers that require more attention, because of a high discrepancies rate. To this end, the homogenisation interface adds the possibility to display mosaics of image and attribute values for arbitrary intervals of as many attributes as desired, an option which was extensively used for checking the stability of each attribute versus time and versus other attributes. The homogenisation process establishes the final and definitive classification of the EFIGI catalogue.

3.4. Representative images of attributes strength

To illustrate the 5 different levels of each attribute, we display in Figs. 3 to 18 the *irg* colour images (see Sect. 2.2) of 3 galaxies for each attribute value (from 0 to 1). For a given attribute

value, we display from top to bottom galaxies of increasing EFIGI Hubble type: the top row shows the commonly called “early-type” galaxies, bulge-dominated (cE, cD, E), lenticulars and S0a; the middle row contains the “intermediate-type” galaxies, that is early spirals, from Sa to Sc; and the bottom row, the “late-type” galaxies containing later spirals, from Scd to Sm, Im and dE. For illustrative purposes, or when none of the types in the 3 categories exist for a given row and attribute value, earlier or later types are shown (in Figs. 4, Figs. 5, 7, 9, 12, 13, 17, 18, and 16).

We emphasise that galaxies shown in Figs. 3 to 16 are not randomly chosen but visually selected from the catalogue, with three goals: 1) to show representative galaxies of each attribute value; 2) to ensure that the wide variety of typical galaxies observed within each EFIGI morphological type are present, and that the different types are equally represented; 3) to display a number of atypical galaxies with the various EFIGI types and attribute values.

For most attributes (except evidently Inclination/Elongation), we show preferentially galaxies with low inclination, as this implies a higher confidence level in most attribute strengths: for example, the presence and strength of spiral arms is difficult and impossible to assess in inclined and edge-on galaxies respectively. We nevertheless show galaxies with all values of the Inclination/Elongation attribute for the Contamination, Multiplicity, Visible Dust, and Dust Dispersion attributes, as these are as or more reliably determined in highly inclined galaxies than in nearly face-on objects.

The typical galaxies shown in Fig. 3-18 include peculiar galaxies which often have a high value of the Perturbation attribute, but also regular galaxies with unusual combinations of attributes, or galaxies in which the attribute is of strikingly high-contrast compared to the rest of the catalogue. For example PGC0042174 in Fig. 12 has a very low B/T ratio for an Sab galaxy; PGC0043733 in Fig. 15 has a remarkably sharp and contrasted bar; PGC0049310 in Fig. 17 has nearly no disk emission between the bar and the inner ring.

3.5. Validation and reliability

We explore the main characteristics and the reliability of the homogenised EHS and the various attributes by comparing the EHS to the RHS, and by examining the trends and dependencies in attributes.

3.5.1. EFIGI-RC3 Hubble sequence comparison

Fig. 19 shows the confusion matrices for the RHS, and the non-homogenised and homogenised EHS classifications. The comparison between both versions of the EFIGI catalogue shows that the non-homogenised catalogue lacks compact galaxies ($T=-6$), and reveals some confusion between ellipticals ($T=-5$) and lenticulars ($T=-3$ to -1). The lower dispersion observed for all types (but cE and dE galaxies) in the right panel compared to the left is proof of a better agreement between the RHS and the EHS after homogenisation of the EFIGI types, thus confirming that this process leads to a more reliable classification. We note that the remarkable level of overall agreement (with the exception of dE types) between the RHS and the EHS classes (despite being produced by different individuals and based on different imaging material) is evidence of the reliability of the Hubble classification for galaxies in the local universe.

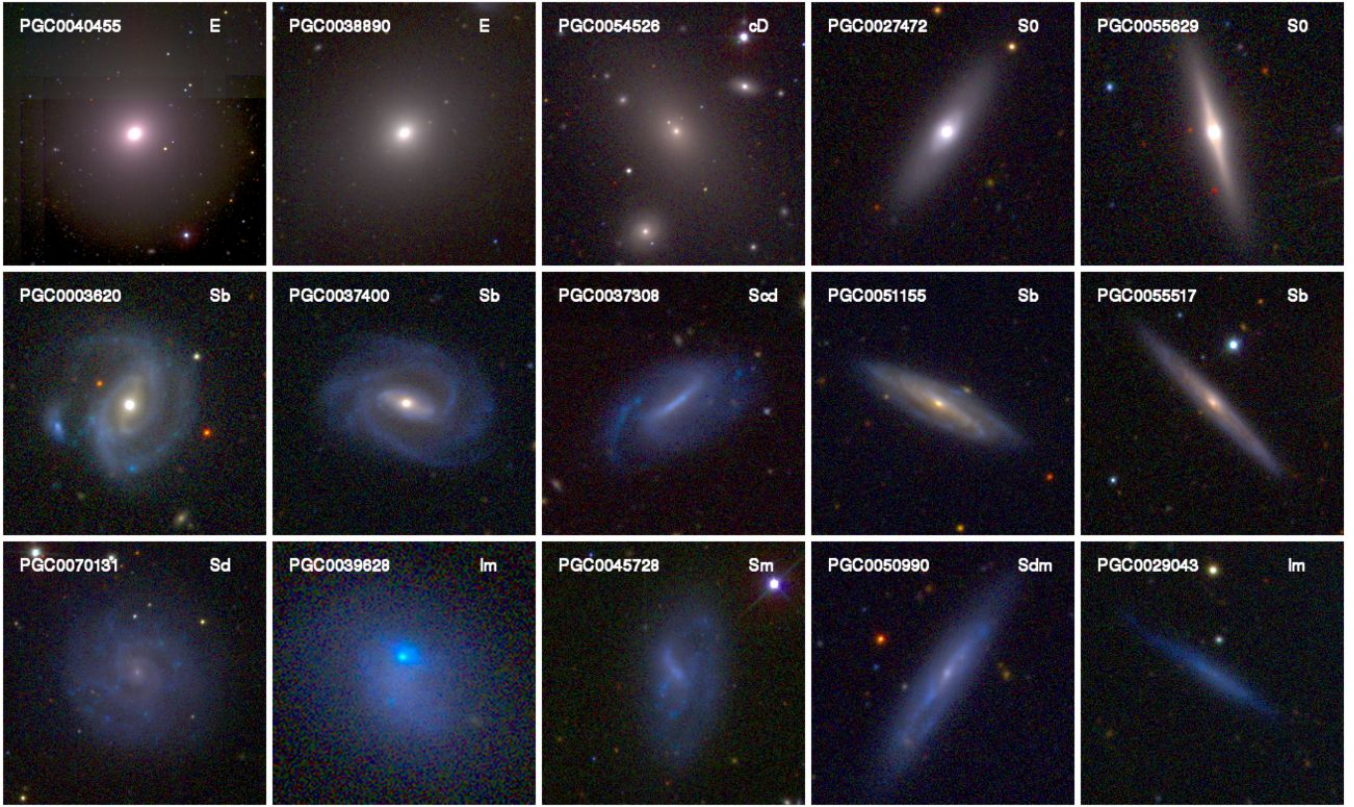


Fig. 3. Examples of EFIGI galaxies with the five possible values of the Inclination/Elongation attribute: 0, 0.25, 0.5, 0.75, and 1 from left to right. The PGC number and the EFIGI Hubble type are indicated inside each image. For each attribute value, 3 types are shown: pure bulge (cE, cD, E), lenticular and S0a galaxies in the top row, early spirals in the middle row (from Sa to Scd), later spirals (Sd to Sm), Im and dE in the bottom row. Note the very low surface brightness of the Scd, Sd, Im and Sm galaxies in the central panel and the 2 left panels in the bottom row, typical of such objects which are numerous in the EFIGI catalogue. In all images, north is up and east to the left.

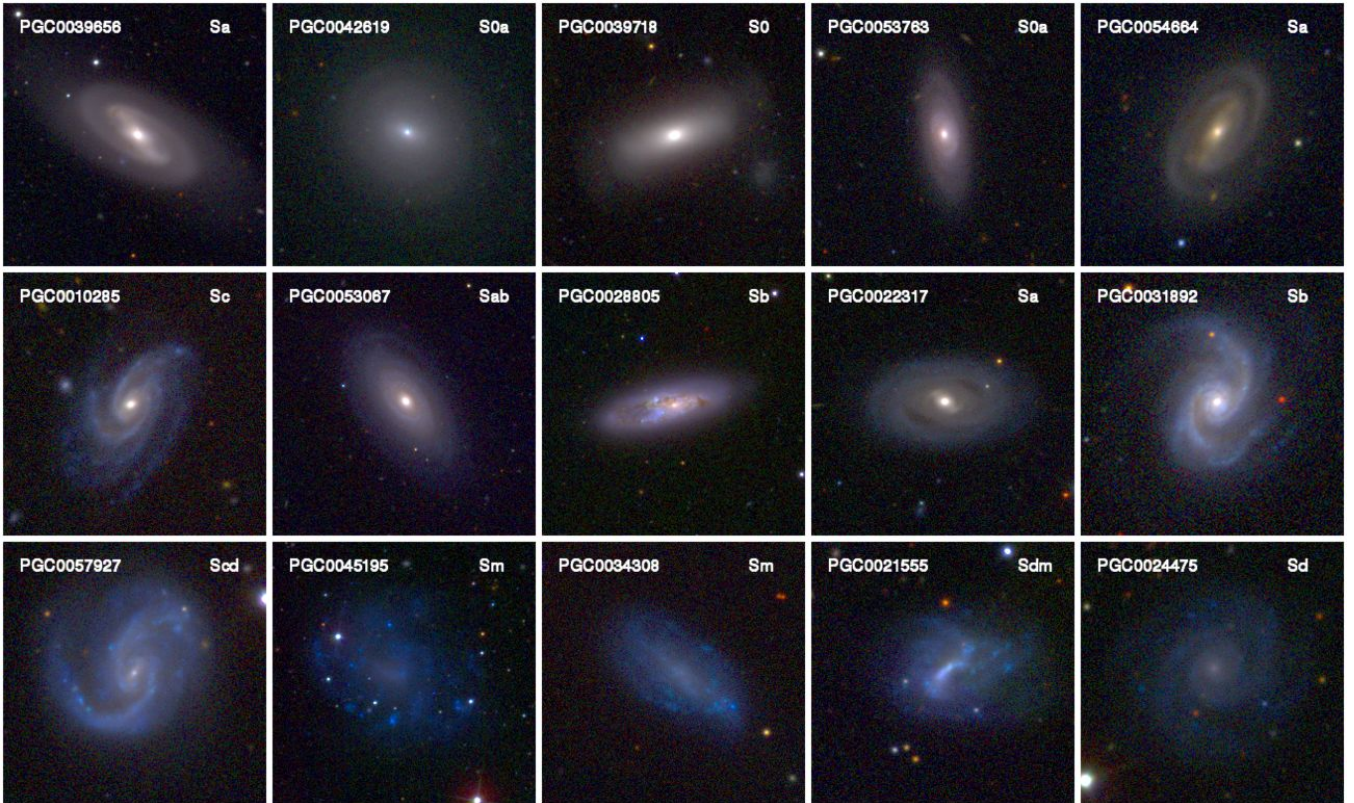


Fig. 4. Same as Fig. 3 for Rotation attribute. The central column containing galaxies having arm-like features but for which no rotation direction can be defined contains unusual galaxies.

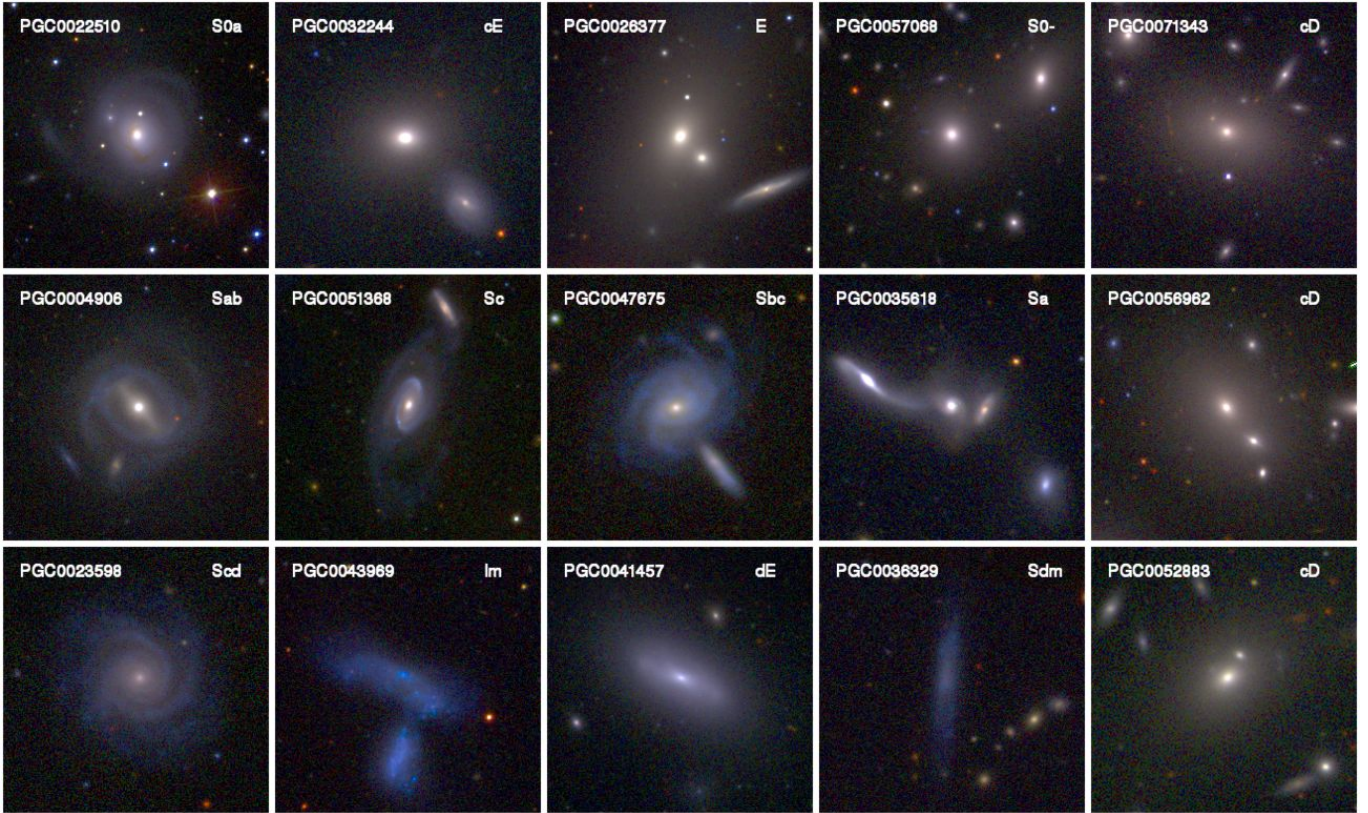


Fig. 5. Same as Fig. 3 for Multiplicity attribute. Because EFIGI galaxies with an attribute value of 0.25 are all cD galaxies, we only display these types in the right panel of each line. As cD galaxies have an extended halo and lie in dense regions of clusters, they have both high Multiplicity attribute and low to moderate Contamination. Note that although PGC0004906 (left panel of central row) has 2 neighbouring galaxies, these are too faint in comparison to the central galaxy to be accounted for in the Multiplicity.

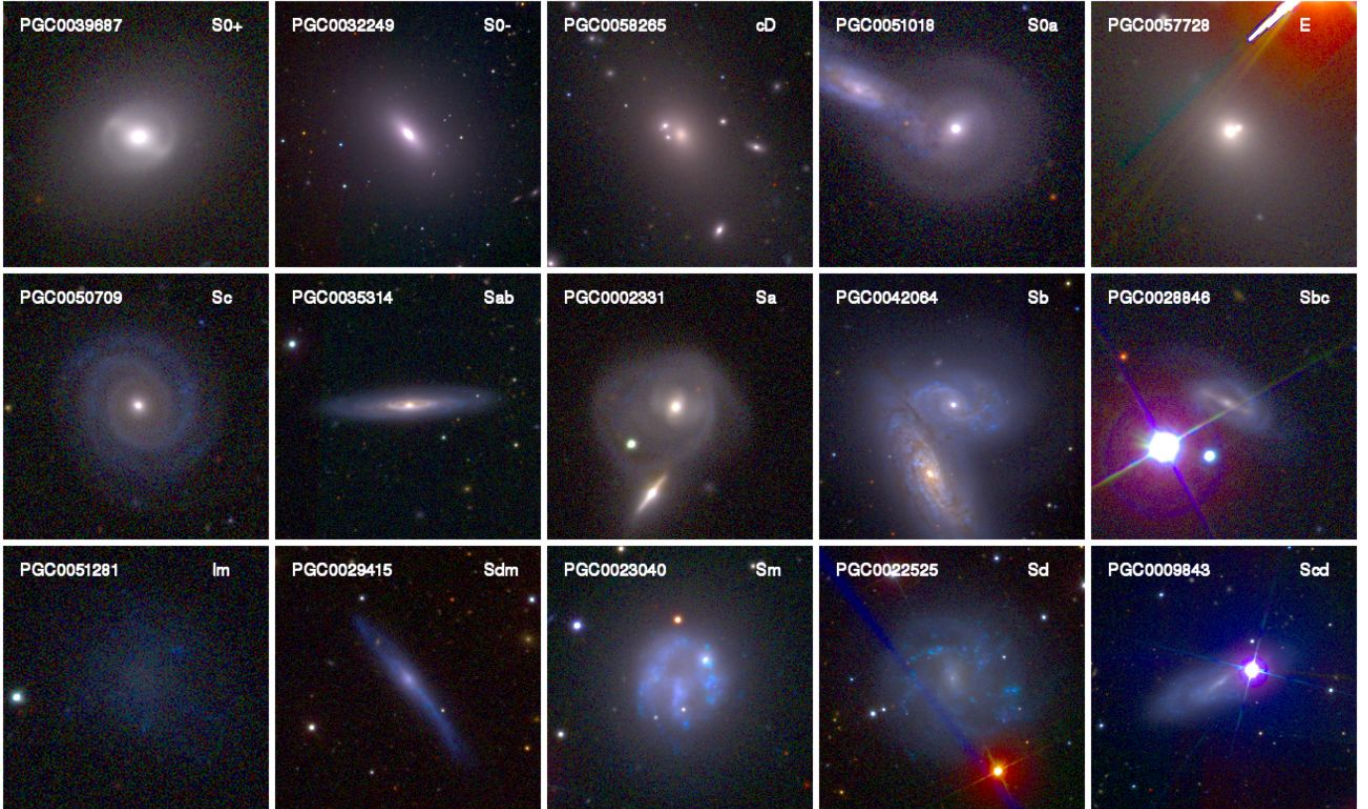


Fig. 6. Same as Fig. 3 for Contamination attribute. Contamination can be due to neighbouring stars, satellite tracks, as well as interacting or overlapping foreground or background galaxies.

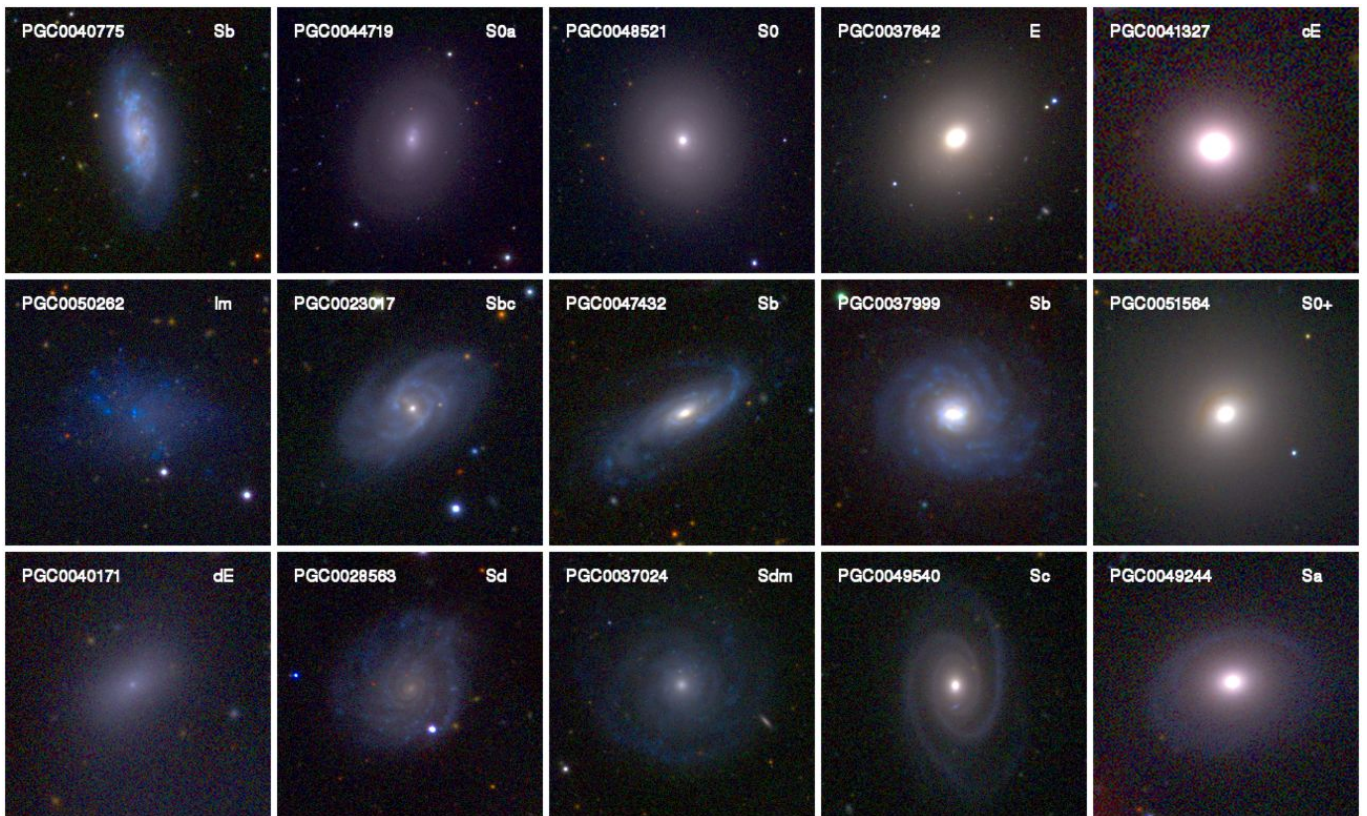


Fig. 7. Same as Fig. 3 for Bulge/Total ratio attribute. Earlier types than Scd are shown in the bottom row for attribute values 0.75 and 1, because later types have lower values of this attribute.

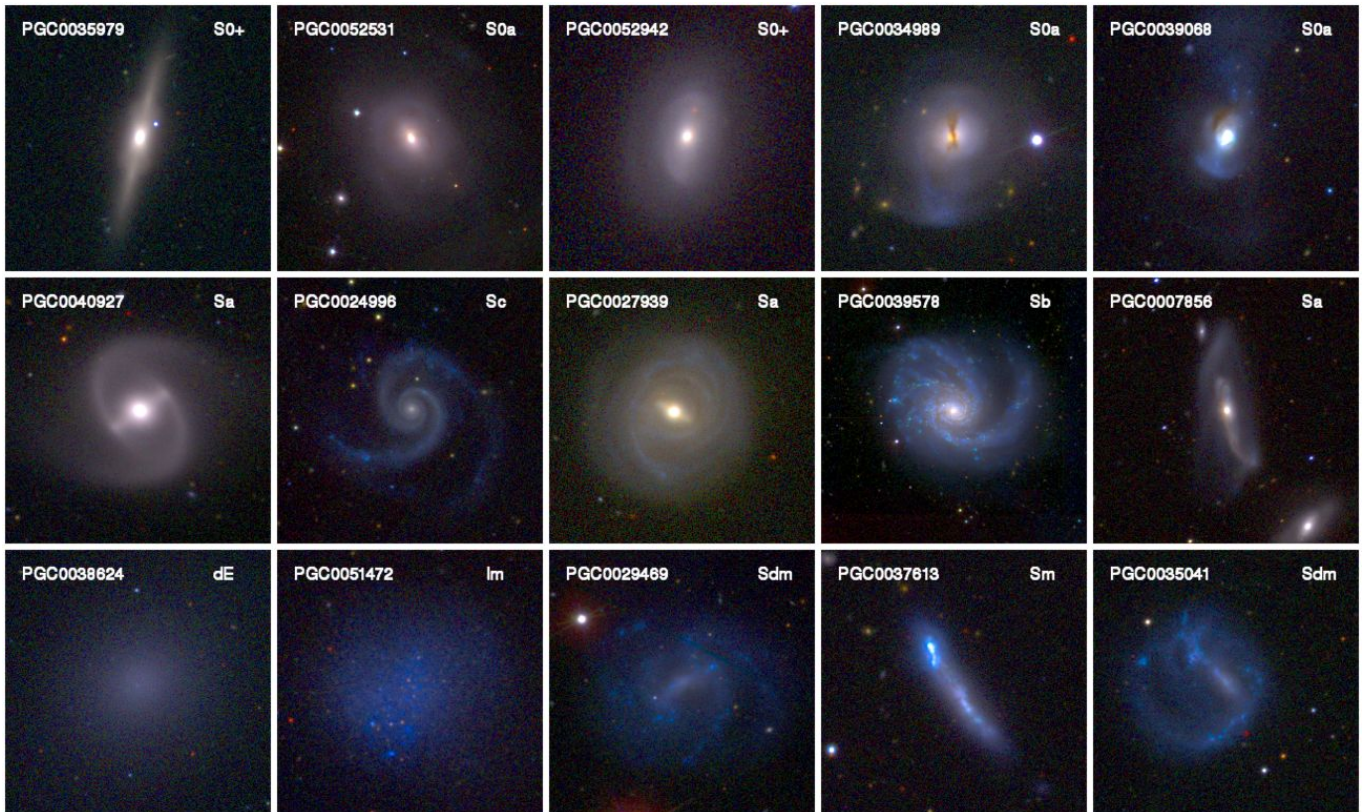


Fig. 8. Same as Fig. 3 for Perturbation attribute. Most dE are unperturbed, whereas many spirals and irregulars are weakly or moderately distorted (attributes values 0.25 and 0.5). Note however the extremely regular nature of the Sa galaxy PGC0040927 (left panel of central row).

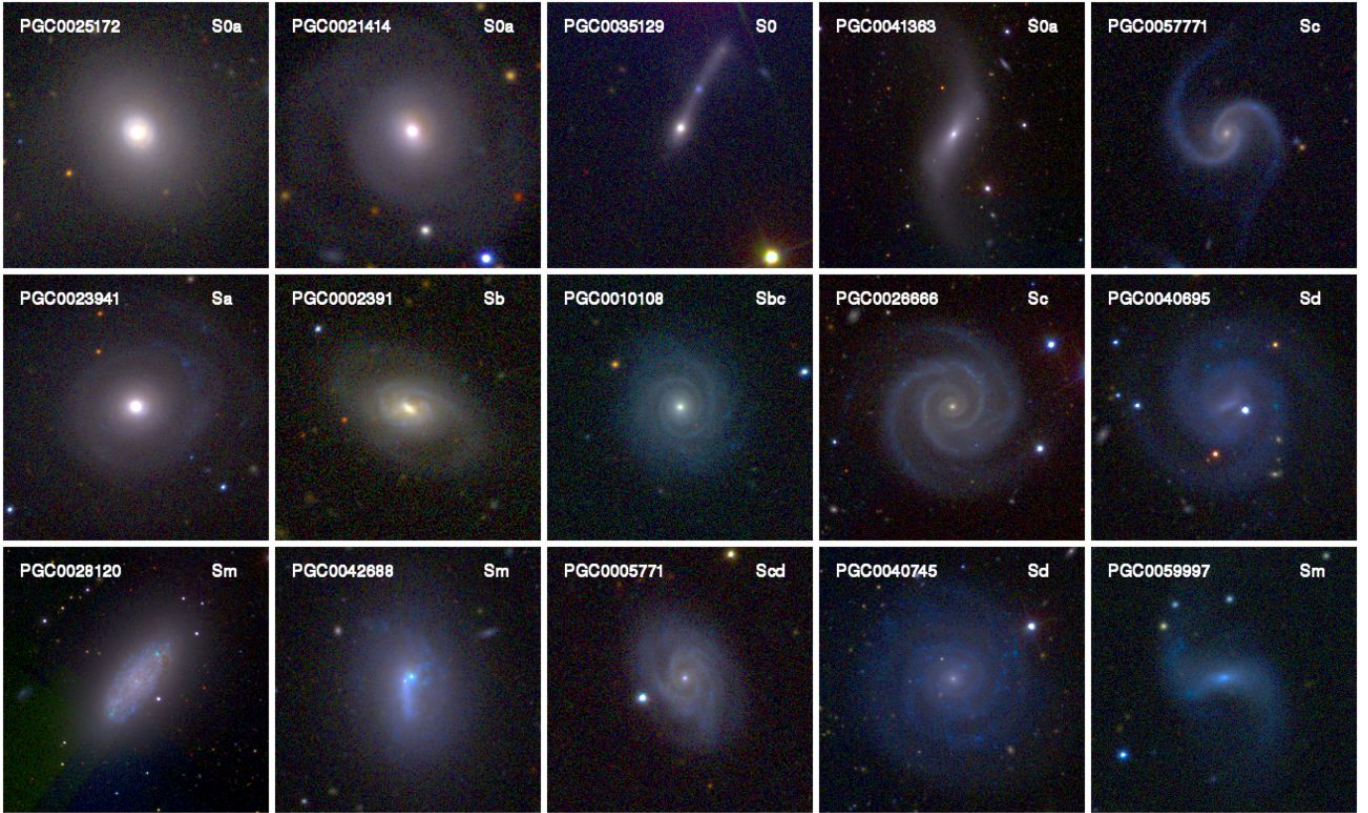


Fig. 9. Same as Fig. 3 for Arm strength attribute. Later types than Fig. 3 are shown in the right panels of the top and central row because all earlier type galaxies have values less or equal to 0.75 for this attribute.

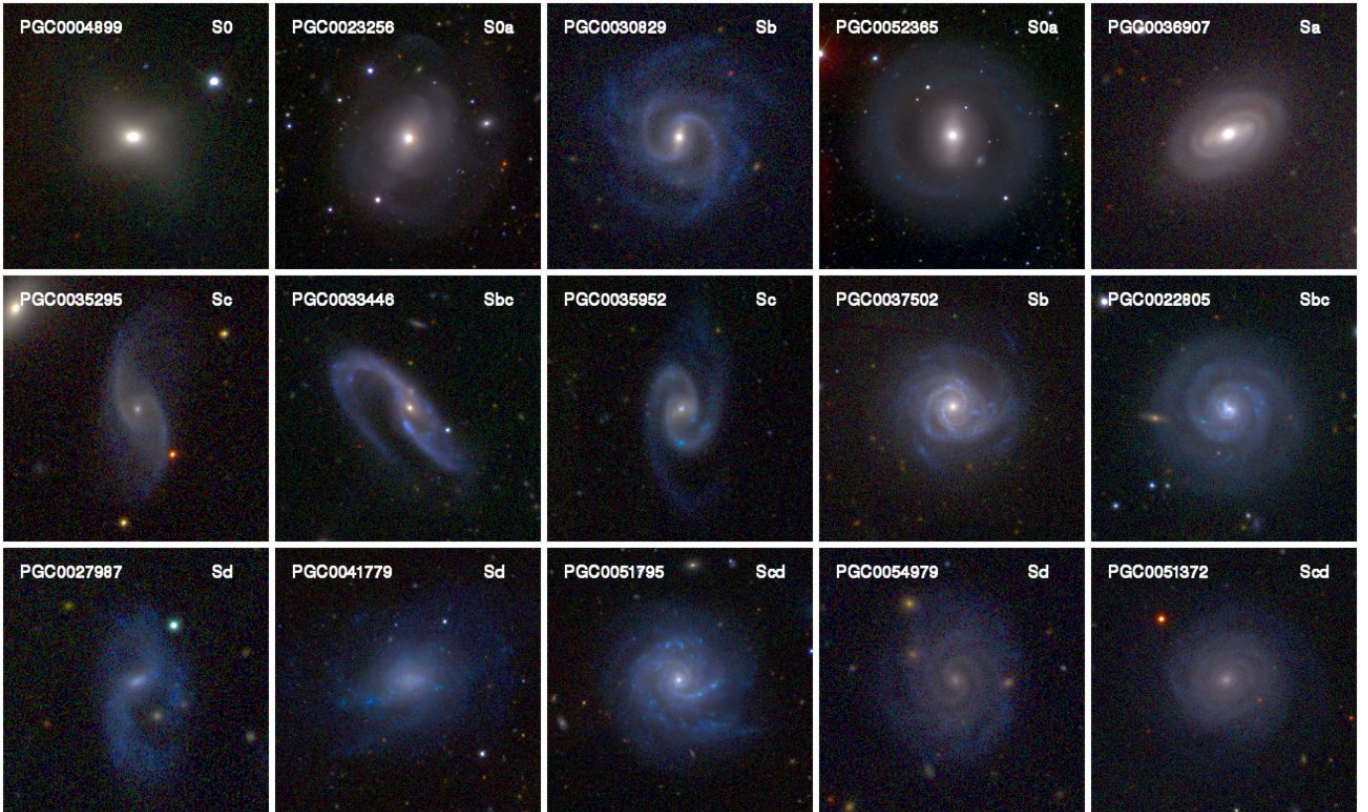


Fig. 10. Same as Fig. 3 for Arm curvature attribute. For most spiral arms, the curvature varies along the arms, and a mean value is estimated for the attribute (see for example PGC0033446, in the central row). Note also the peculiar cross-like shape of lenticular galaxy PGC004899 in the left panel of upper row.

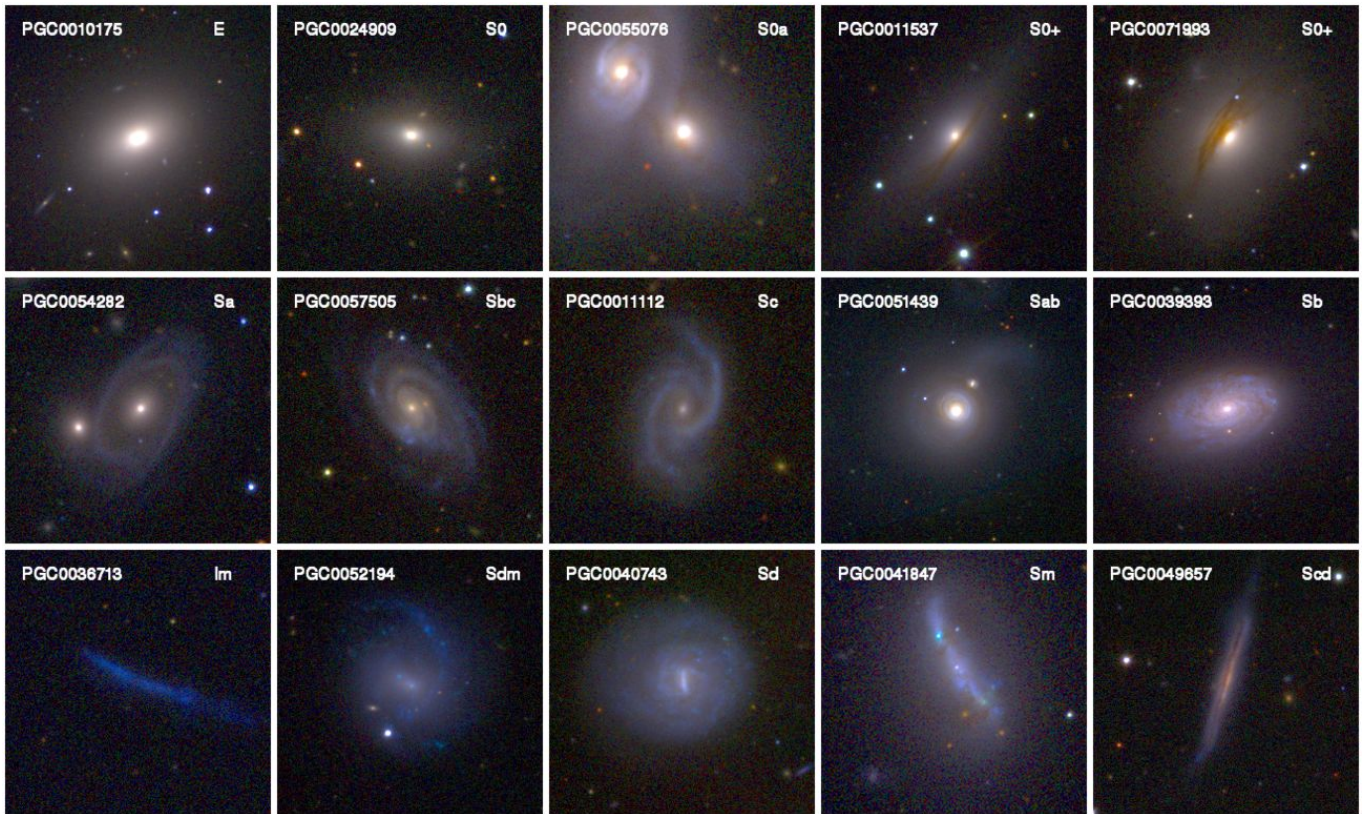


Fig. 11. Same as Fig. 3 for Visible dust attribute. Most spiral galaxies contain dust, even in low amounts, and galaxies with high amounts of dust are often perturbed, as illustrated by PGC0071993 (top row), PGC0039393 (central row) and PGC0041847 (bottom row).

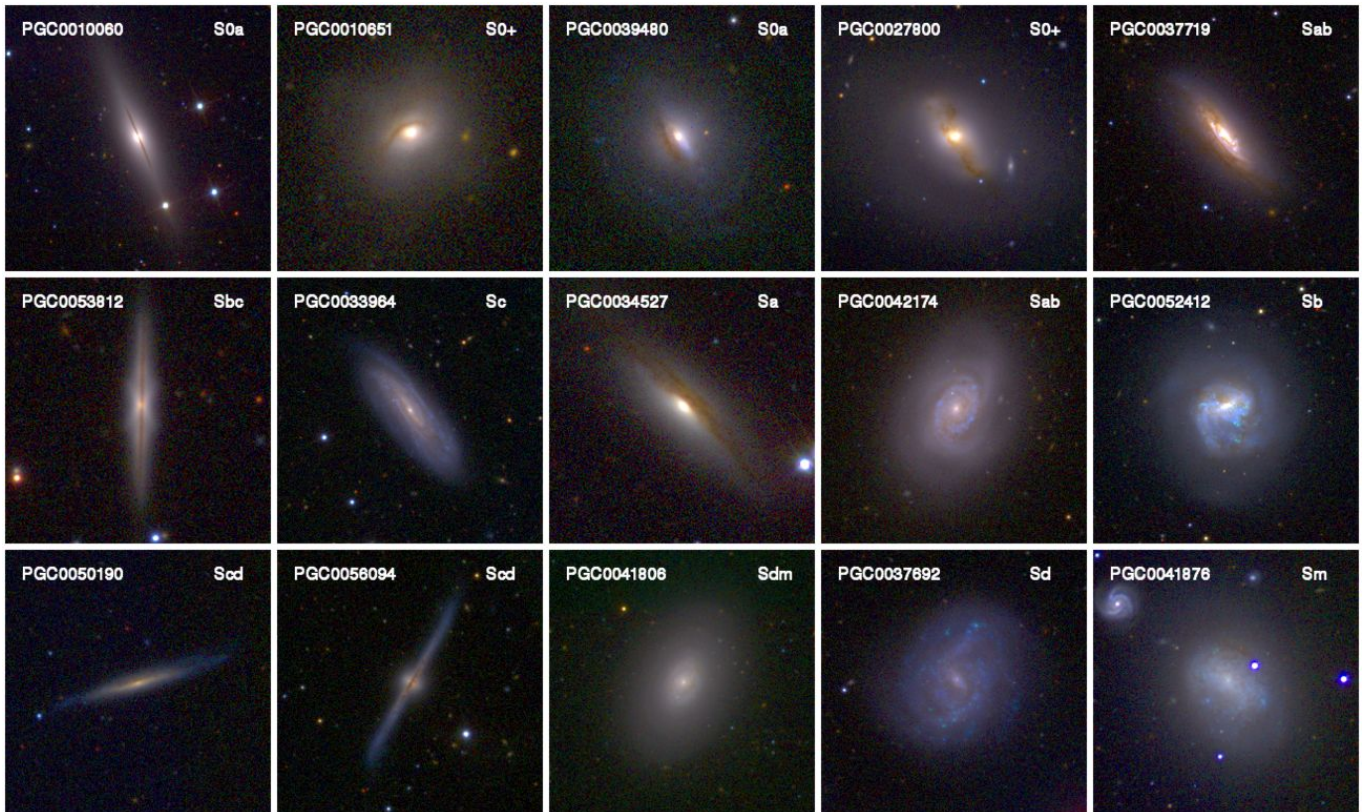


Fig. 12. Same as Fig. 3 for Dust dispersion attribute. PGC0037719 in the top right panel is the earliest type galaxy (Sab) with an attribute value of 1. The low values of the Dust dispersion attribute are preferentially seen in highly inclined galaxies, as indicated by the anti-correlation between both attributes in Fig. 20. Note the unusually faint bulge of Sab galaxy PGC0042174 (central row, second from the right).

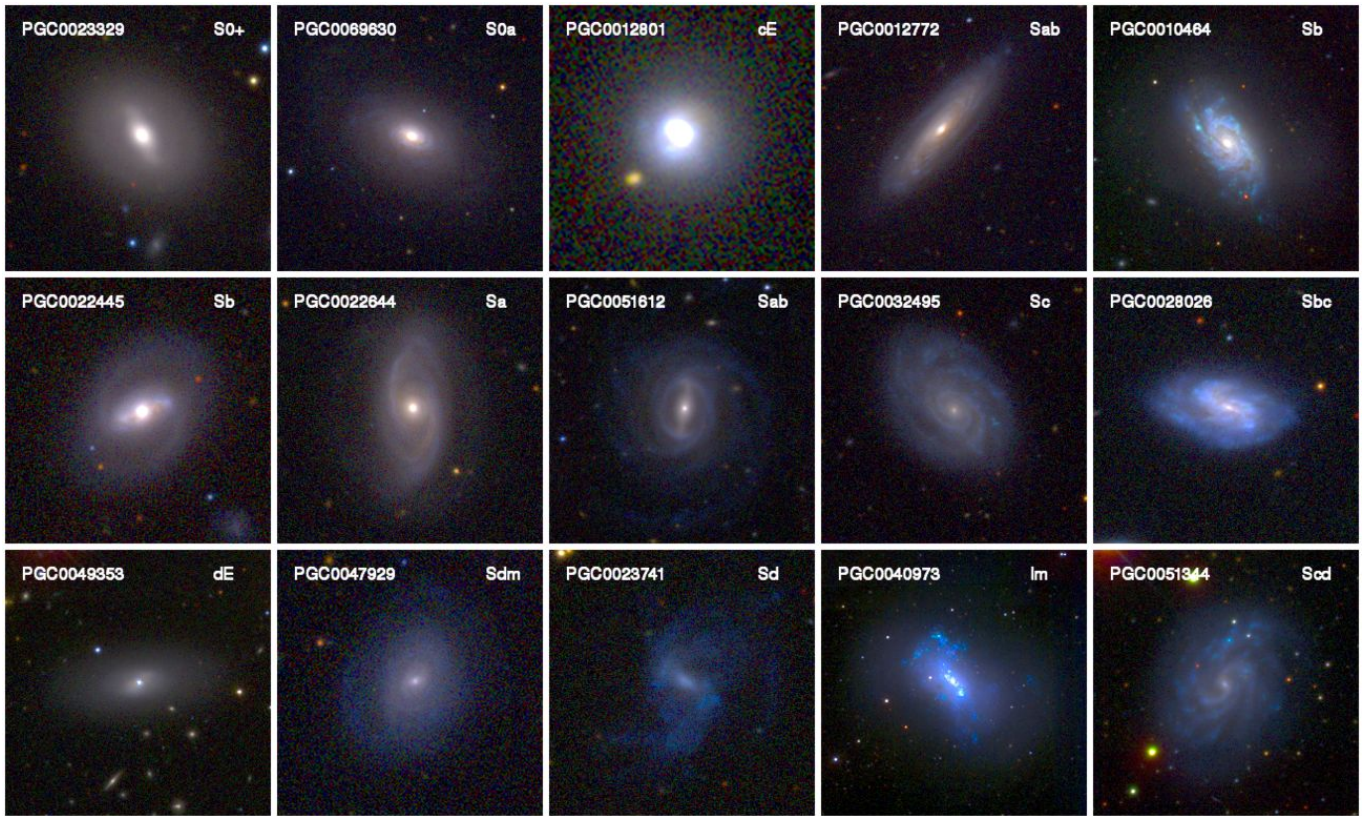


Fig. 13. Same as Fig. 3 for Flocculence attribute. Sab and Sb galaxies (PGC0012772 and PGC0010464) are shown in the top row because there are no galaxies of earlier type with an attribute value of 0.75 or 1. We show in the left panel of the bottom row a nucleated dwarf lenticular galaxy classified as dE in the EFIGI catalogue, which has no flocculence; it however has an Hot Spot attribute value of 0.5 due to an unusually strong nucleus.

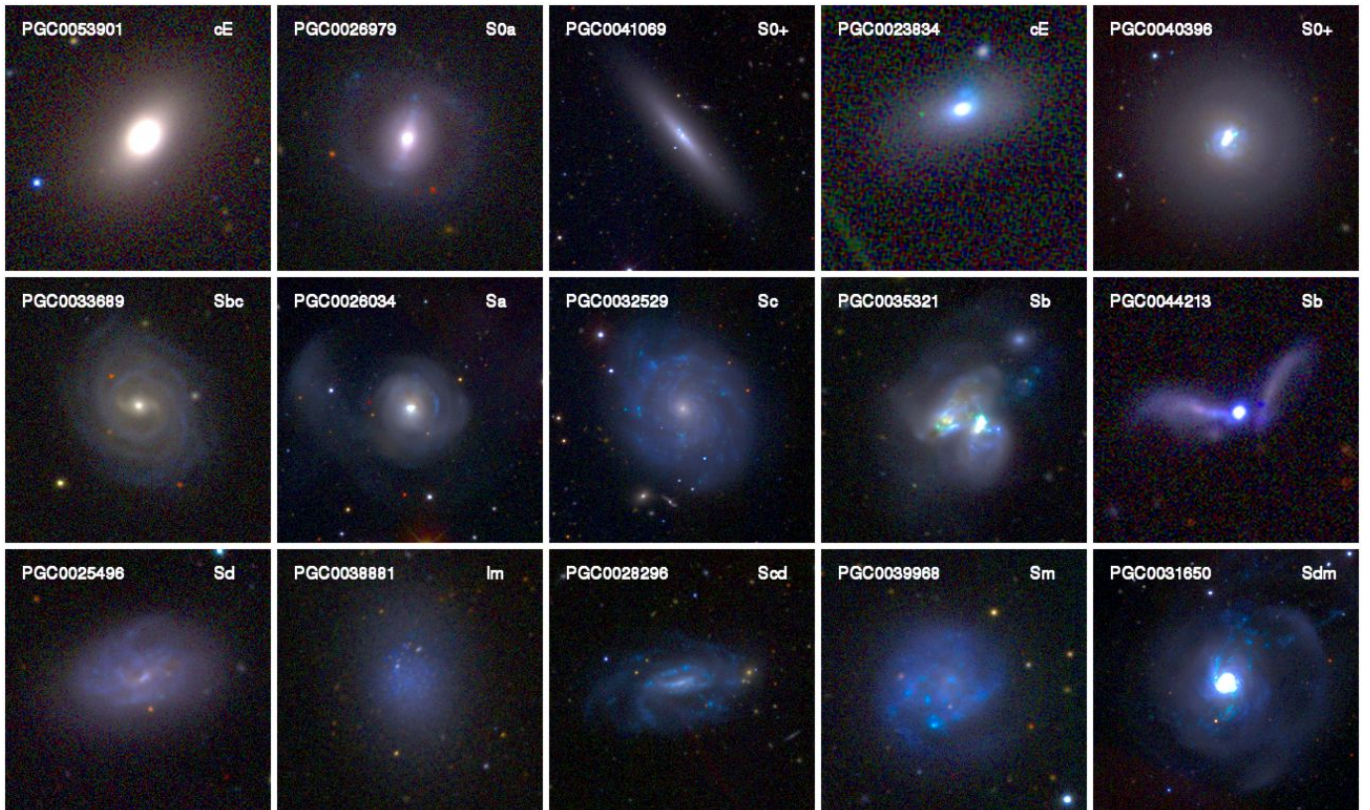


Fig. 14. Same as Fig. 3 for Hot spots attribute. As seen here, strong values of the attribute (2 right columns) often implies strong values of the Perturbation attribute; this is also measured by the strong correlation between both attributes in Fig. 20.

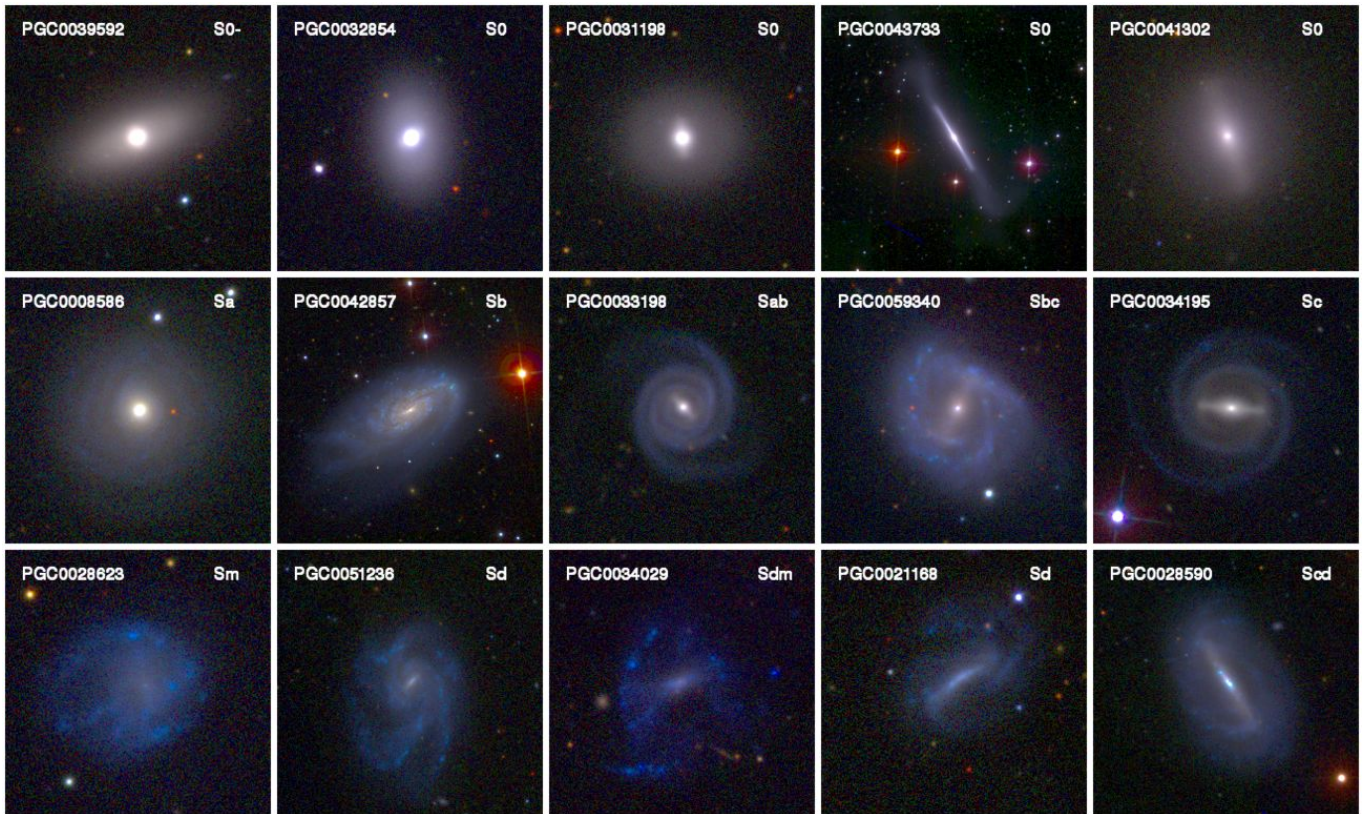


Fig. 15. Same as Fig. 3 for the Bar length attribute. Bars are frequent in all galaxy types except cE, cD, ellipticals and dE. PGC0059340 (second panel from the right in the central row) illustrates that a bar can be long, hence a high attribute value of 0.75, but with a low surface brightness.

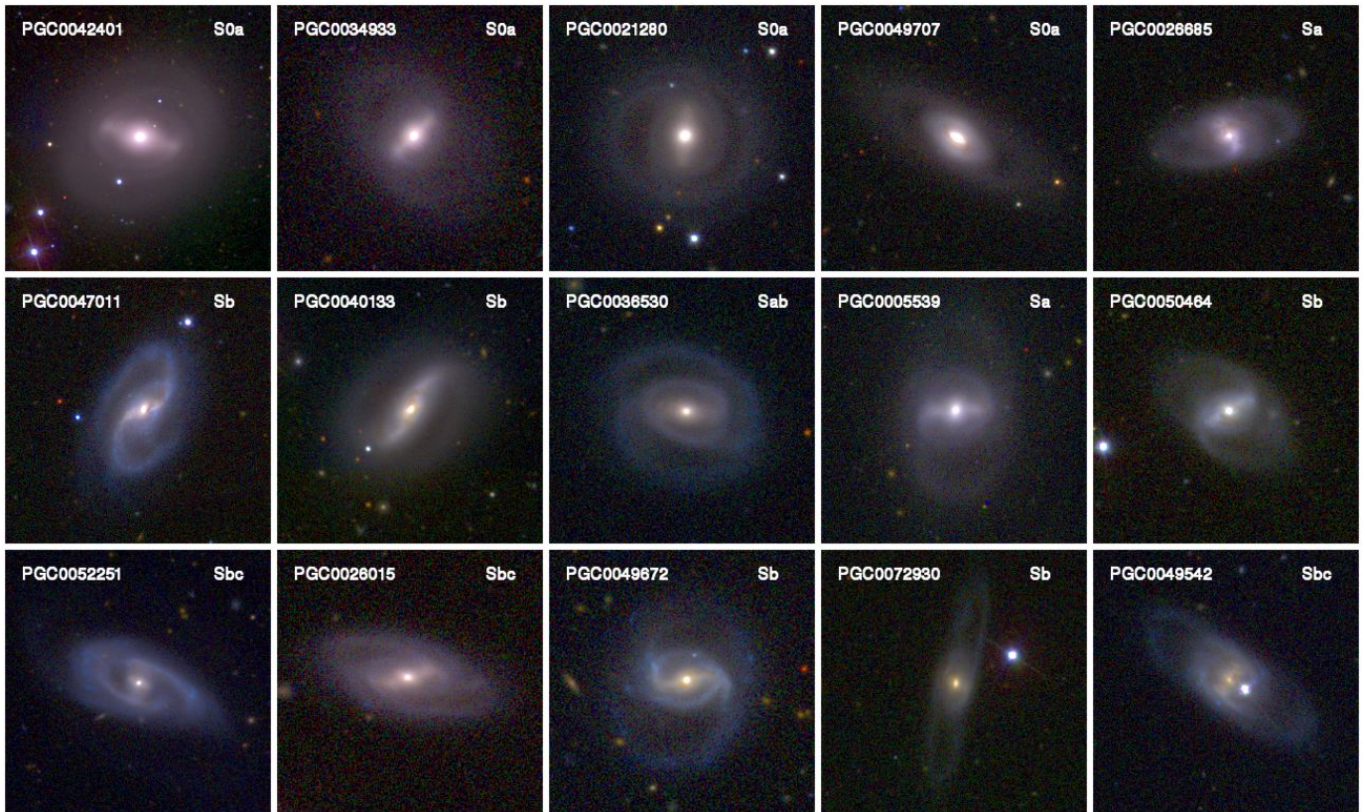


Fig. 16. Same as Fig. 3 for Pseudo-Ring attribute. As this is a low surface brightness feature, high-contrast pseudo-rings are preferentially shown here. The galaxies shown in the bottom row are the latest type galaxies (Sbc, Sb, Sb, Sbc resp.) with attributes values of 0.25, 0.5, 0.75, 1.0 respectively (for a fair comparison, an Sbc galaxy is also shown in the bottom row for attribute value 0).

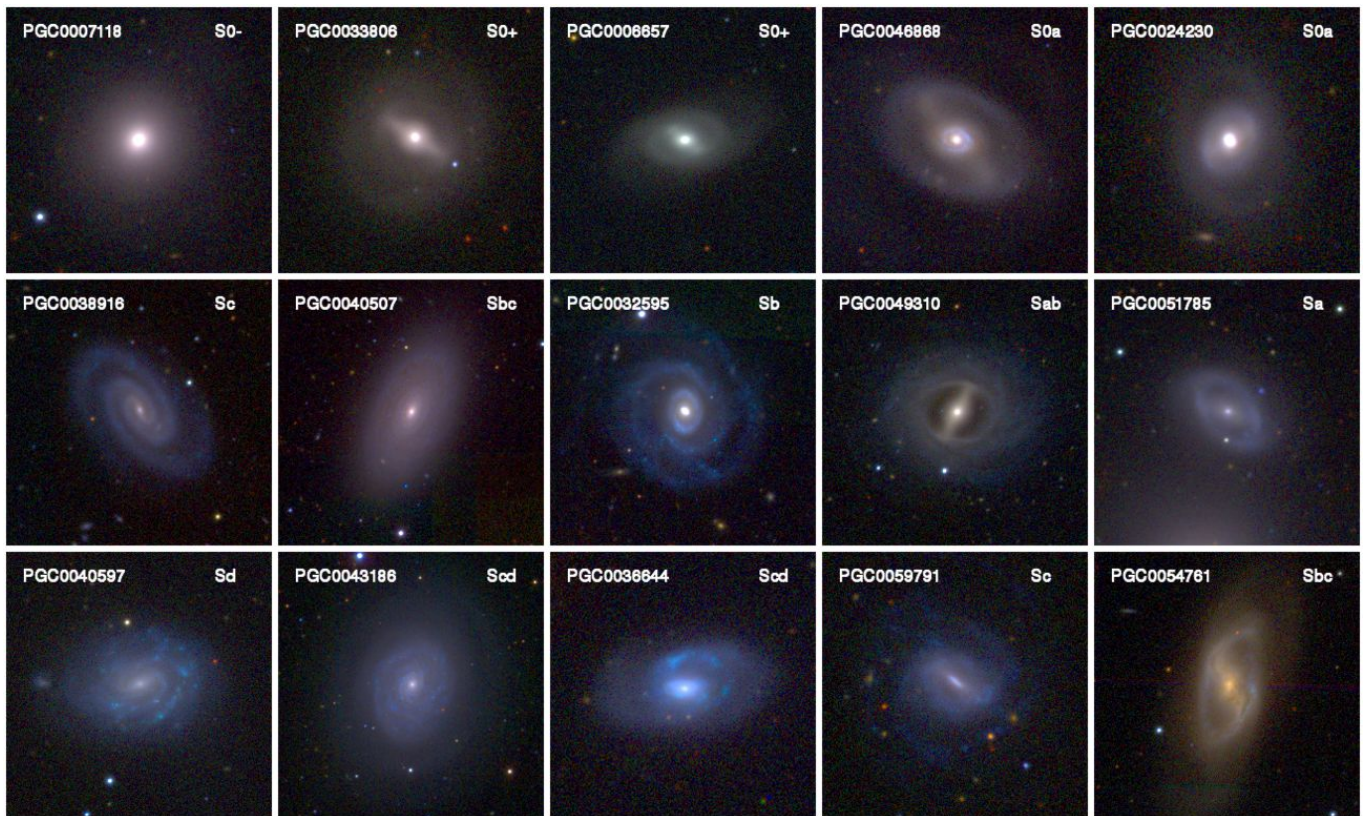


Fig. 17. Same as Fig. 3 for Inner Ring attribute. PGC0059791 and PGC0054761 (2 right panels in the bottom row) are the latest type galaxies (Sc and Sbc resp.) with a strong and very strong Inner Ring respectively. In PGC0046868 (second panel from the right in the top row) the Inner Ring attribute points to the ring encircling the bar; the additional blue ring inscribed within the bar is a “nuclear ring”, not characterised here.

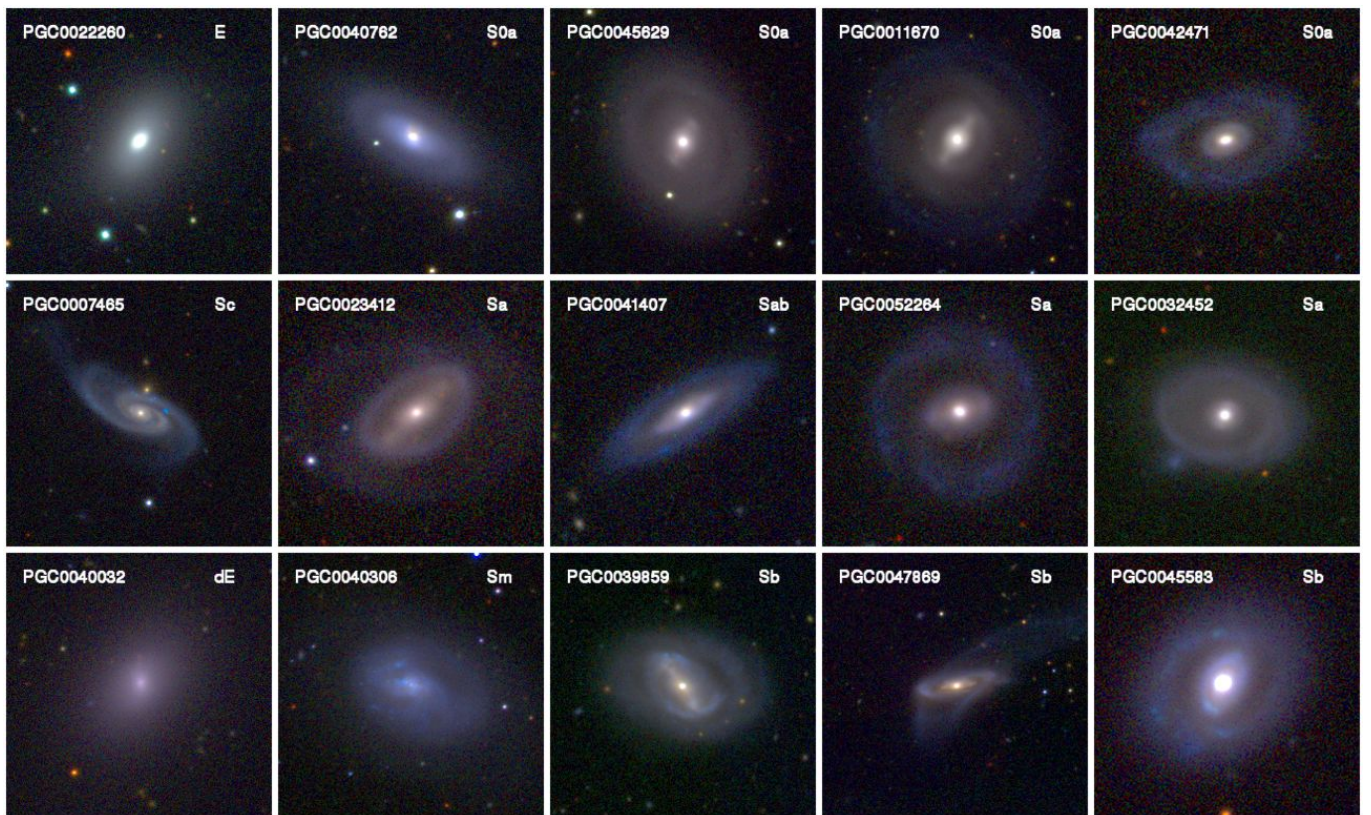


Fig. 18. Same as Fig. 3 for Outer Ring attribute. As some outer rings can be of very low surface brightness, we preferentially show here galaxies with high-contrast rings. PGC0039859, PGC0047869 and PGC0045583 (3 right panels in the bottom row) are among the latest type galaxies (Sb) with values of the Outer Ring attribute between 0.5 and 1.

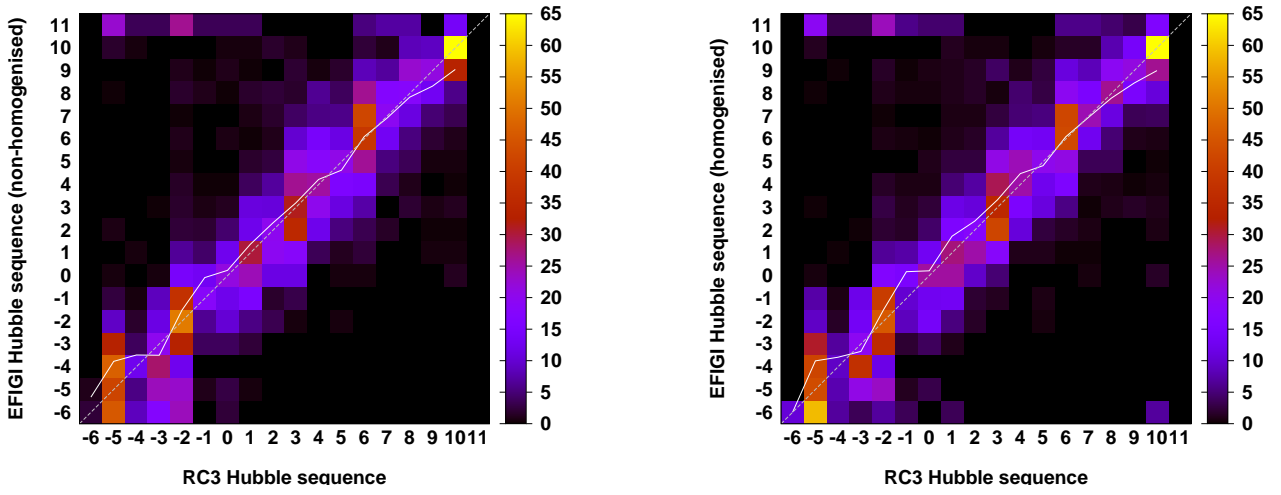


Fig. 19. Confusion matrices between the RC3 Revised Hubble Sequence (RHS) and two versions of the EFIGI Hubble sequence: before (*left*) and after homogenisation (*right*). The dash-dotted line along the diagonal corresponds to a perfect match. The solid white line connects the average EFIGI type in each PGC type bin.

Pseudo-ring																													
Outer ring																+0.20													
Inner ring															+0.34	+0.27													
Bar length															+0.43	+0.10	+0.18												
Hot spots															+0.12	-0.10	-0.06	-0.04											
Flocculence															+0.70	+0.27	+0.08	-0.03	-0.02										
Dust dispersion															+0.57	+0.36	-0.09	-0.19	-0.09	-0.05									
Visible dust															+0.21	+0.63	+0.20	+0.21	+0.18	+0.02	+0.05								
Arm rotation															-0.05	-0.13	-0.09	-0.04	+0.04	+0.01	+0.02	+0.03							
Arm curvature															+0.01	+0.36	-0.00	-0.16	-0.37	-0.10	+0.25	+0.23	+0.09						
Arm strength															+0.01	-0.05	+0.59	+0.22	+0.74	+0.35	+0.35	+0.11	-0.07	-0.05					
B/T															-0.31	+0.48	+0.02	-0.06	-0.29	-0.67	-0.59	-0.14	+0.18	+0.11	+0.06				
Perturbation															-0.41	+0.29	-0.43	-0.01	+0.23	+0.27	+0.54	+0.63	+0.17	-0.02	-0.02	-0.05			
Contamination															+0.10	+0.12	-0.10	-0.06	+0.03	-0.08	+0.01	-0.15	+0.00	-0.09	+0.00	-0.00	+0.02		
Multiplicity															+0.31	+0.09	+0.14	-0.10	-0.06	+0.00	-0.05	-0.02	-0.14	-0.07	-0.12	-0.03	-0.03	-0.02	
Inclination															-0.04	-0.14	-0.14	-0.24	-0.08	-0.05	-0.02	+0.29	-0.25	+0.04	-0.14	+0.02	-0.05	-0.02	-0.00
	Inclination	Multiplicity	Contamination	Perturbation	B/T	Arm strength	Arm curvature	Arm rotation	Visible dust	Dust dispersion	Flocculence	Hot spots	Bar length	Inner ring	Outer ring	Pseudo-ring													

Fig. 20. Confusion matrices (in grey levels) and Pearson's correlation coefficients for attribute pairs in the homogenised data set. Correlation coefficients higher than 0.2 are coloured in red, while those lower than -0.2 are in green.

3.5.2. Dependencies among attributes

Fig. 20 shows the weighted confusion matrices and Pearson's correlation coefficients for all pairs of morphological attributes. The strongest correlations are found between *flocculence* and the *hot spots* (+0.70) and *arm strength* (+0.74) attributes. *Visible dust* is also strongly correlated to *flocculence* (+0.63), and *arm strength* (+0.59). Taken together, these correlations probably reflect the fact that *flocculence*, *hot spots* and *visible dust* are related indicators of the level of star formation activity in a galaxy. These attributes are correlated with *arm strength*, presumably because star formation is enhanced in the spiral arms due to gas compression by density waves. The *perturbation* attribute is also strongly correlated with both *hot spots* (+0.63) and *flocculence* (+0.54), hinting that tidal and merging processes enhance star formation in galaxies.

The strongest anti-correlations are found between *B/T ratio* and the *flocculence* (-0.67) and *hot spots* (-0.59) attributes. Strong anti-correlations with *B/T ratio* are also measured when considering *perturbation* (-0.41), *arm strength* (-0.31), and *dust dispersion* (-0.29). All these anti-correlations reflect the increasing strength of the aforementioned attributes along the Hubble sequence, along with the *B/T ratio* which gradually decreases, as shown in de Lapparent et al. (2011). The strong correlation observed between *B/T ratio* and *arm curvature* (+0.48) is consistent with the winding of spiral arms being a major criterion for defining the progression of spiral types along the Hubble sequence (van den Bergh 1998).

The correlation between the presence of a bar and that of an inner ring noticed by Kormendy (1979) and Hunt & Malkan (1999) is clearly seen in the EFIGI catalogue (+0.43). Some level of correlation is also found between *inner ring* and *outer ring* (+0.34), and between both attributes and *pseudo-ring* (+0.27 and +0.20 resp.). The presence of a *pseudo-ring* often implies that of an *inner ring*, and the full range of transition stages between an *outer ring* and a *pseudo-ring* is present in the EFIGI catalogue. These various correlations are further examined in the companion article reporting on the statistical analysis of the EFIGI attributes (de Lapparent et al. 2011). These effects were already pointed out by Buta & Combes (1996), who discuss rings in terms of barred galaxy models.

The various correlations and anti-correlations between the EFIGI *inclination/elongation* attribute and the *B/T ratio*, *visible dust* and *dust dispersion* attributes resp. are difficult to interpret as they may partly originate from a type effect, pure bulge galaxies having higher fractions with *inclination/elongation* = 0 or 0.25 than disk galaxies (see de Lapparent et al. 2011).

3.5.3. Trends in attribute strength

The EFIGI catalogue is vulnerable to possible trends arising from a modification of the perception of the astronomer during the long time periods (weeks) spent at classifying and homogenising individual attributes. Visual examination has often been conducted by increasing PGC number, which is itself ordered in right ascension. Although this approach makes it much easier to identify galaxy pair components and spot duplicates, it also makes the detection of trends more ambiguous because of the well-known correlation between galaxy morphology and density (Dressler 1980; Postman & Geller 1984).

To examine whether there are systematic drifts with time in the homogenised EFIGI attributes, we plot in Fig. 21 the sky distribution of the local weighted average of attribute strengths. This graph does show some significant peaks, which can be attributed to galaxy clusters (Fig. 22), but reassuringly no significant “banding” pattern is visible in right ascension.

The mean *B/T* increases near to clusters because of the local over-density of early type galaxies. This is particularly apparent in the Hercules cluster. The increase is less pronounced in Virgo as it is close enough for a number of dwarf elliptical galaxies with disk-like profiles to enter the sample and somewhat compensate the excess number of early-type galaxies (the majority of the EFIGI dEs are located in Virgo). Apart from those peaks, global trends seems to be well behaved, at least below the 10% level.

4. PSF estimates

Knowledge of the image Point Spread Function (PSF) is essential to most morphometric measurements, in particular those involving models adjustments. The PSFs of the EFIGI images were measured on the same combined “fPc” SDSS DR4 images rescaled around each galaxy, as in Sect. 2.2 but without clipping to 255x255 pixels. The wider field of view provides typically a hundred point-sources suitable to PSF modelling. We used the PSFEX software⁸ Bertin et al. (in prep.) which generates a tabulated model with adaptive sampling and achieves super-resolution when the input data are undersampled, which is the case for a large fraction of the EFIGI images because of the angular rescaling. For simplicity, we ignored the spatial variations of the PSF around each galaxy. PSF variations within the field of view are indeed expected for the most extended objects as a result of combining exposures obtained under different conditions; however downscaling makes the PSF so sharp for these objects that the consequences are negligible.

5. Overall properties of the catalogue

5.1. Sky coverage

Fig. 22 shows the projected distribution of EFIGI galaxies onto the sky. The solid angle covered by the EFIGI catalogue corresponds to the SDSS photometric DR4, 6670 deg².

5.2. Cluster detection

A systematic search for clusters and groups is performed to trace environment effects in the present analysis (see Fig. 21 and the related section) and in future works. A list of clusters in the area covered by EFIGI catalogue is retrieved using the NED “all-sky” query form for redshifts $0.001 < z < 0.05$ and richness above 50. For each cluster listed, we count the number of EFIGI galaxies within a limited volume around the cluster. We build a “box” centred on right ascension, declination and redshift of the cluster with dimensions equal to 1 Mpc × 1 Mpc × 2.000 km s⁻¹. We assume $H_0 = 73 \text{ km s}^{-1} \text{ Mpc}^{-1}$ (Freedman et al. 2001). Concentrations with more than 5 EFIGI galaxies within the search box are added to the list of EFIGI clusters. Clusters identified using this procedure are overplotted as a red dot surrounded by red circles onto the sky distribution of EFIGI galaxies in Fig. 22; the circle size indicates the relative cluster richness extracted from NED. We find 10 clusters in the EFIGI catalogue,

⁸ <http://astromatic.net/software/psfex>

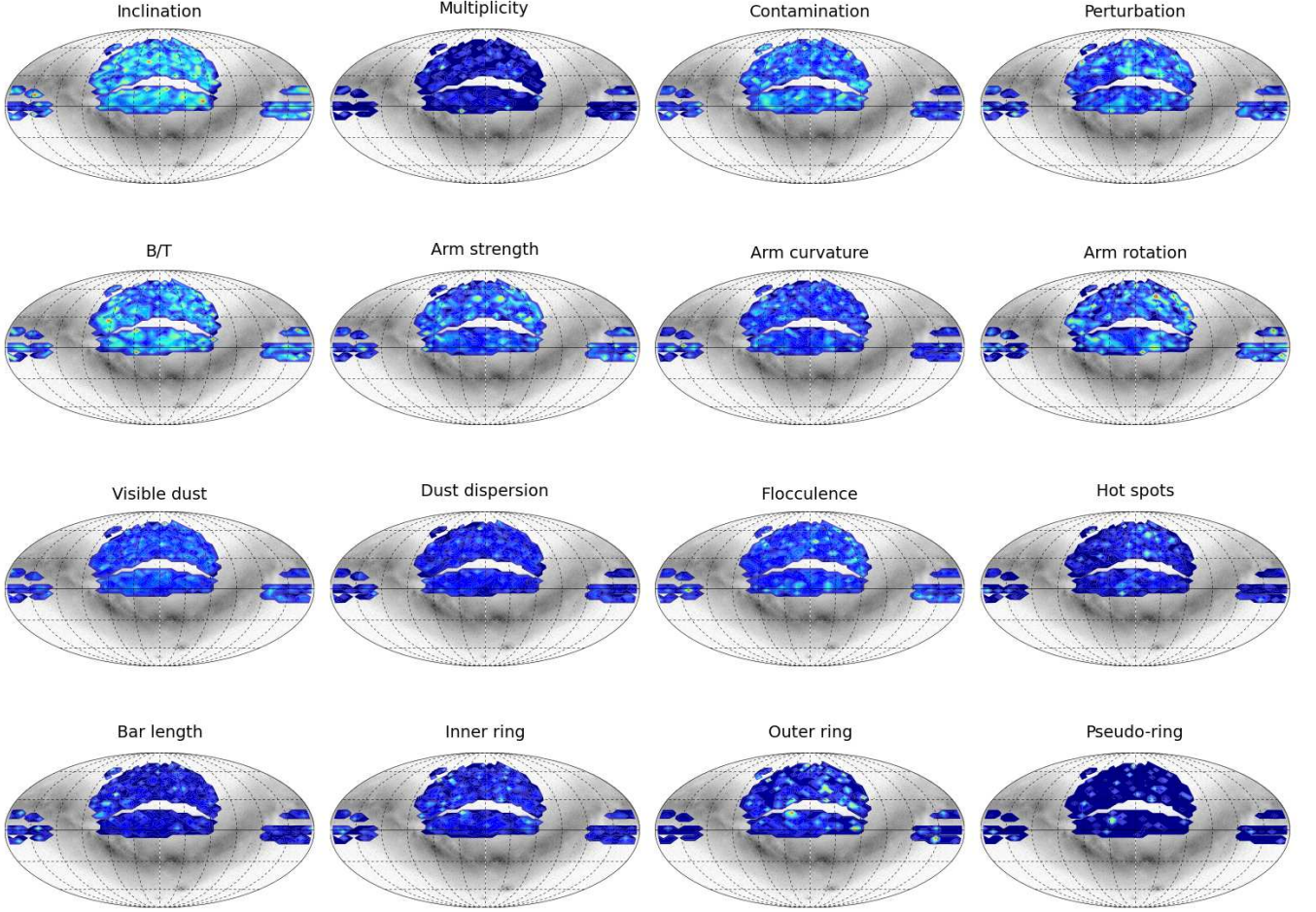


Fig. 21. Angular distribution of weighted average attribute strengths in the EFIGI catalogue. Right ascension runs right to left from 0^h to 24^h (see Fig. 22). The weight is set to 0 for confidence intervals $\Delta x = 1$, and $(\Delta x + 0.25)^{-2}$ otherwise (see Sect. 3.2). The colour scale is relative and runs from dark-blue to green, yellow, and red for the highest values.

which indeed correspond to over-densities of galaxies in the projected map of Fig. 22. Other visible over-densities may be due to chance projections.

5.3. Magnitude distributions

Fig. 23 shows for each SDSS filter the distribution of SDSS Petrosian magnitudes for all EFIGI galaxies by intervals of 0.5 magnitude. A bright bell-shaped distribution with an extension fainter than magnitude $\sim 17 - 19$ is seen in all five filters. We interpret this extension as a consequence of erroneous flux measurements, likely due to the splitting of large galaxies into several fainter and smaller objects by the SDSS pipeline. SDSS photometric measurements are unreliable for objects larger than $\sim 1 - 2$ arcmin. Among the 4458 EFIGI galaxies, 257 have no measured major isophotal diameter D_{25} in the RC2 system (de Vaucouleurs et al. 1976), 954 have D_{25} below 1 arcmin, 2444 between 1 and 2 arcmin and 811 above 2 arcmin. Fig. 23 also shows that a large fraction of objects in the extensions are late spiral types, as indicated by histograms restricted to EFIGI galaxies with types Sd and later. This magnitude extension is not seen in the distribution of PGC B_T magnitudes in Fig. 23, which shows instead a sharp cut-off. Additional support for this

interpretation comes from the two magnitude brighter extension of the B_T distribution at bright magnitudes compared to that of SDSS g measurements (see Fig. 23).

This photometric discrepancy is further illustrated in Fig. 24, which shows the magnitude difference between the PGC B_T band and the SDSS Petrosian g band for the various EFIGI types of the 1006 galaxies with a B_T magnitude. The graph shows a high dispersion in the SDSS g magnitudes for all values of PGC B_T , with a significant tail towards flux underestimation in the SDSS by up to 8 magnitudes. Galaxies with magnitude differences of more than 2 magnitudes in Fig. 24 are mostly of types Sd to Im, in agreement with the excess splitting of these objects illustrated in Fig. 23.

5.4. Photometric completeness

We extracted from the SDSS DR4 all objects in the “Galaxy” catalogue that do not have the “SATURATED” flag. This flag indicates that an object includes one or more saturated pixels, and allows the removal of a large proportion of stars included in the “Galaxy” catalogue ($\sim 30\%$ at $g \leq 18$). However, we include objects located near the edge of the SDSS CCD frames (with the “EDGE” flag), which is true for $\sim 2 - 3\%$ of EFIGI

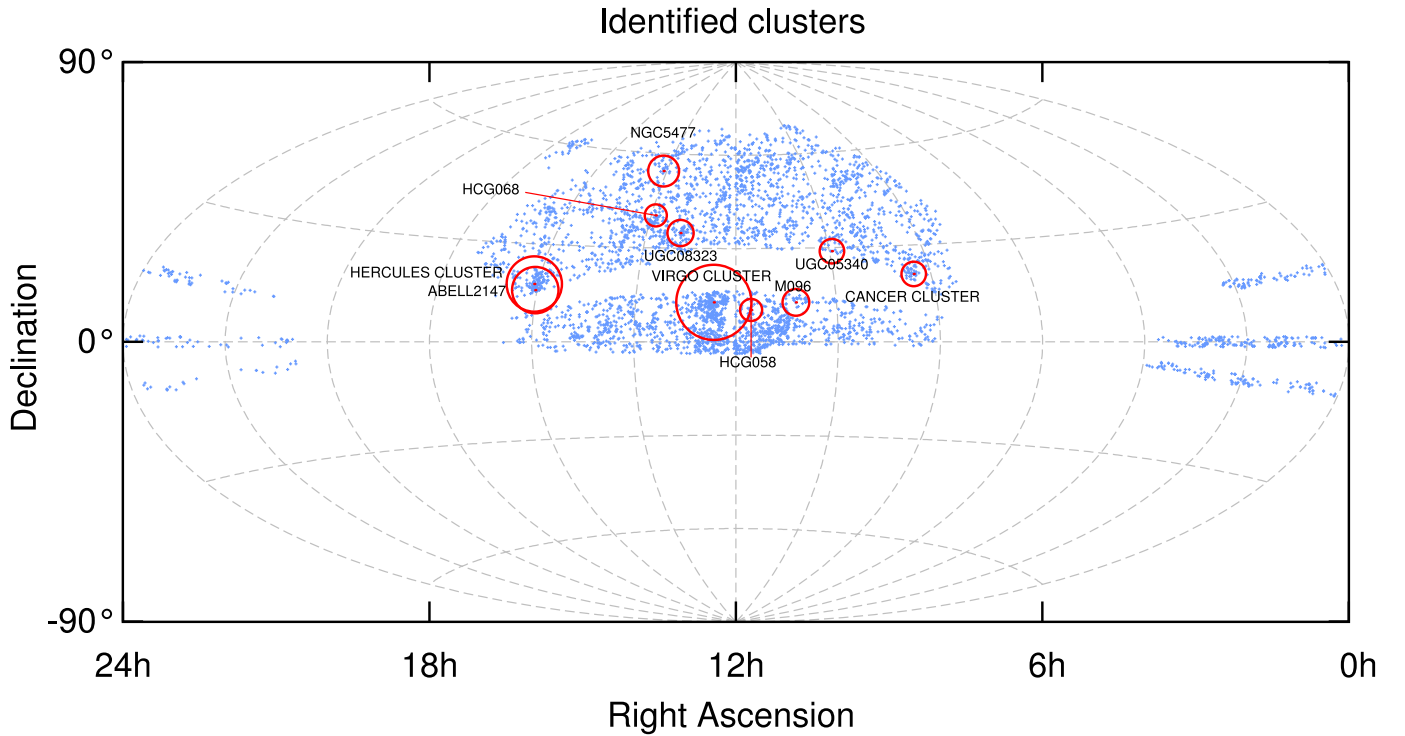


Fig. 22. Blue points are EFIGI galaxies. Red circles indicate clusters and are centred on NED cluster coordinates. The enclosed area is proportional to the number of cluster members as reported by NED.

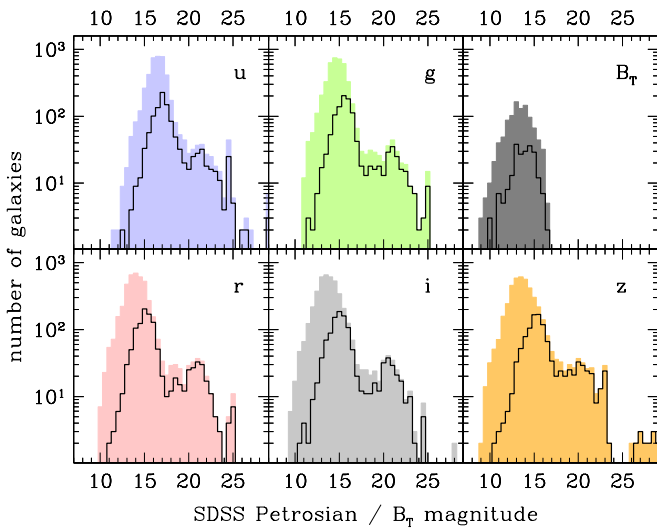


Fig. 23. Shaded histograms show the distribution of SDSS Petrosian magnitudes for EFIGI galaxies in the u , g , r , i and z bands in intervals of 0.5 magnitude (2 upper left panels, and bottom panels), and the distribution of the PGC B_T magnitude for the 1006 EFIGI galaxies for which it is available (upper right panel). In each panel, the black lines shows the histograms restricted to galaxies of types Sd and later. All panels for SDSS magnitudes show an extension to faint magnitudes (enhanced by the logarithmic scale), caused by the limitations in the processing of large objects by the SDSS photometric pipeline.

galaxies. These SDSS samples are selected in Petrosian magnitude, with a limit of 20 in u and 18 in the other bands, in order to sample the bright peak of the EFIGI magnitude distributions (see Fig. 23); beyond these limits, the number of galaxies in the SDSS increases steeply and the completeness drops to 0.

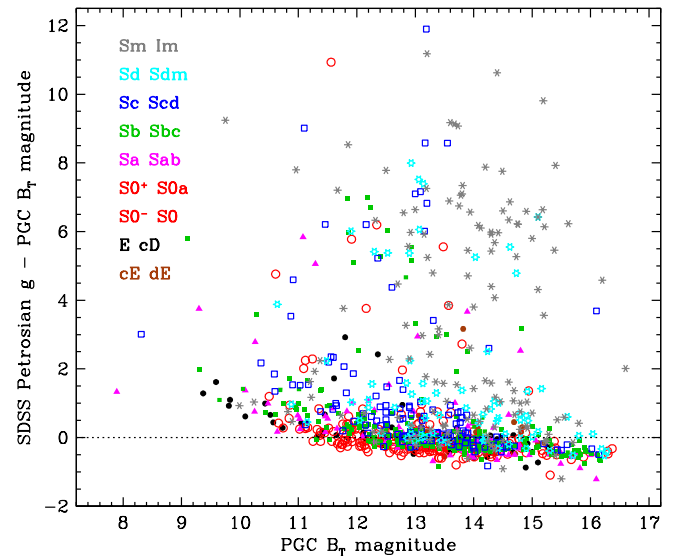


Fig. 24. Comparison between the PGC B_T and the SDSS Petrosian g magnitudes, showing a high dispersion from the splitting of large galaxies in the SDSS photometric pipeline.

Before calculating the photometric completeness, we exclude the 56 EFIGI galaxies that were not identified in the SDSS magnitude limited samples (see Sect. 2.3). We also exclude EFIGI galaxies flagged as “SATURATED” in the SDSS database. These galaxies either have a bright core with some likely saturated central pixels, or contain a contaminating or nearby bright star (as confirmed by the EFIGI contamination attribute), or have the “COSMIC_RAY” flag indicating that the object contains a pixel interpreted to be part of a cosmic ray.

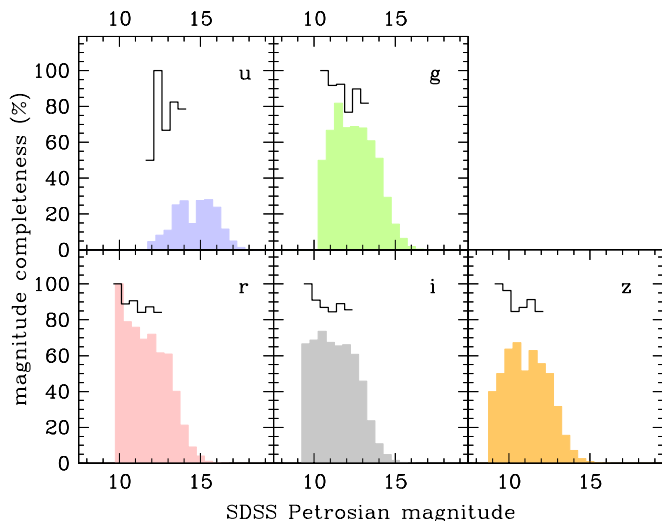


Fig. 25. Shaded histograms show the magnitude completeness of the EFIGI catalogue compared to the SDSS DR4 samples excluding objects flagged as “SATURATED”. All EFIGI galaxies not included in the DR4 comparison samples have been removed (see text for details). The apparent 30-60% completeness is largely an underestimate due to numerous artefacts (halos of bright stars, satellite trails, faint compact objects) included in the DR4 sample. The bright part of the corrected completeness curves are shown as solid lines; note that the brightest bin of the u corrected curve with 50% completeness contains a single EFIGI galaxy.

This removes another 570, 252, 754, 634, and 544 EFIGI galaxies that are not included in the $u \leq 20$, $g \leq 18$, $r \leq 18$, $i \leq 18$, and $z \leq 18$ SDSS sub-samples respectively.

The magnitude completeness in each sample is calculated as the ratio of the number of EFIGI galaxies to that in the SDSS using 0.5 magnitude intervals. The resulting curves for the 5 SDSS filters are shown as shaded histograms in Fig. 25, indicating median completenesses of $\sim 30\%$ in u , and $\sim 60 - 70\%$ in g , r , i , and z .

These curves however largely underestimate the EFIGI completeness. We have examined visually (using the SDSS DR7 “Explore” tool) 890 of the brightest SDSS sources in all 5 filters which are not included in the EFIGI catalogue. Only 95 were found to be a bright galaxy with the stated Petrosian magnitude in the considered band. One third of the other 795 sources are small compact objects (faint stars or galaxies), some of which are in the USNO catalogue. These objects have faint SDSS “psf” magnitudes of 20 to 22 in the r filter, and their Petrosian magnitudes are contaminated by the background halo of bright stars. The remaining two-thirds are spurious objects caused by the halos of bright stars and satellite trails. The apparently low completeness ($\leq 30\%$) in u is due to an even higher number of spurious sources in this filter than in the other bands. This illustrates that the SDSS catalogues are not appropriate for making a complete census of nearby galaxies. A clean reanalysis of the images is necessary.

We overplot in Fig. 24 as continuous black lines the corrected EFIGI completeness curves after removing the aforementioned 795 spurious sources from the SDSS. Because the number of both real and spurious SDSS sources increases steeply at fainter magnitudes, these corrected curves are only measured for their first 5 to 6 bins, and indicate completenesses of $\sim 80\%$ in the u and g filters, and $\sim 85\%$ in the r , i , and z filters. These find-

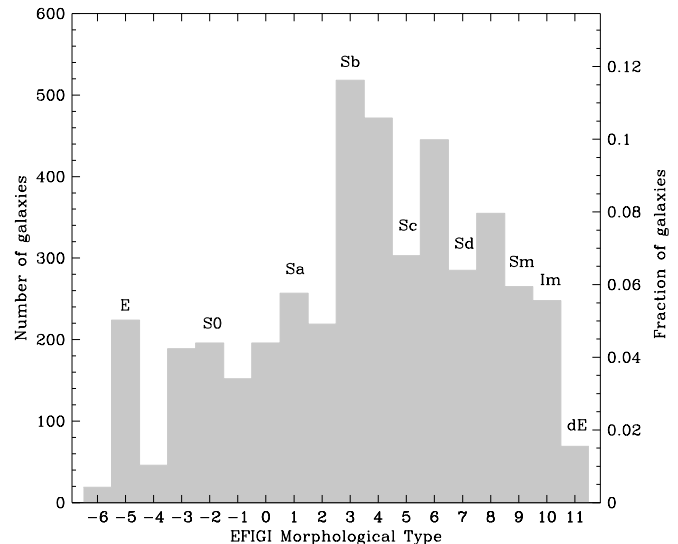


Fig. 26. Distribution of EFIGI morphological types for all 4458 galaxies.

ings lead us to conclude that the EFIGI catalogue is reasonably complete down to $g \sim 14$.

We checked that the estimated DR4 completenesses are also valid for the SDSS DR7 final release. To this end, we made the same extractions from the DR7 as from the DR4 (all objects from the “Galaxy” catalogue that do not have the “SATURATED” flag). Depending on the filter, the DR7 contains about 55% to 75% more galaxies than the DR4 to the same Petrosian magnitude limits. This is due to an increased sky coverage: there are about 10 additional thin strips and also the part of the northern galactic cap region near the declination interval 10° to 30° missing in the DR4 which is now covered (see Fig. 22). In the common area of the DR4 and DR7, both releases have similar magnitude distributions. The stated completenesses of the EFIGI catalogue in the $ugriz$ filters are therefore also valid for the DR7 within the area covered by the DR4.

5.5. Morphological fractions

Fig. 26 shows the numbers and fractions of EFIGI galaxies with each EFIGI morphological type. This graph shows that the late-type Sd, Sm and Im galaxies are as numerous as Sa and Sc types, with $\sim 250 - 300$ galaxies per type; Sb and intermediate types Sbc, Scd, and Sdm have even more galaxies per type ($\sim 350 - 450$); only cD, cE and dE types, which are intrinsically rare or faint have $\sim 20 - 70$ galaxies. This is further shown in Fig. 27 where we plot the fractions of galaxies grouped by type as a function of redshift. At redshifts $z < 0.02$, the Sd, Sdm, Sm and Im galaxies represent $\sim 41\%$ of the sample.

The EFIGI sample is not a volume-limited sample. de Lapparent et al. (2011) show that it is essentially limited in apparent diameter, as measured by D_{25} (de Vaucouleurs et al. 1976), following the RC3 selection criterion (de Vaucouleurs et al. 1991). It is nevertheless interesting to compare the distribution of morphological types in the EFIGI catalogue with that expected from a magnitude-limited sample, since setting a magnitude cut-off is the most common selection scheme in morphological follow-up studies of photometric surveys (Lintott et al. 2008; Nair & Abraham 2010).

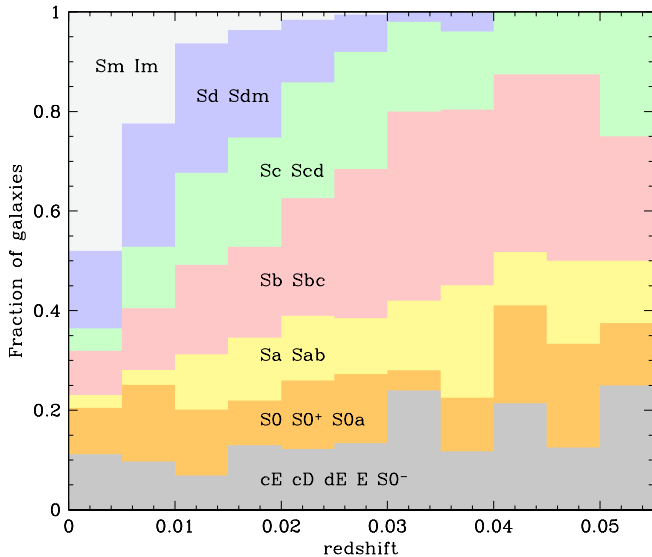


Fig. 27. Fraction of EFIGI galaxies with a given morphological type as a function of redshift.

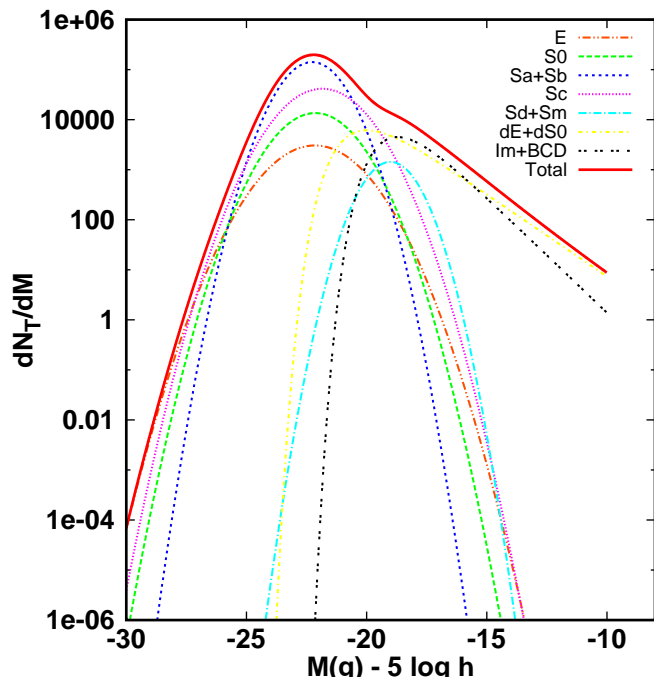


Fig. 28. Expected numbers of galaxies with $g < 15.75$ per unit of absolute V band magnitude within the survey volume of the EFIGI catalogue (see text).

We compute the fractions of galaxies by morphological type from the luminosity functions (LFs hereafter) listed in de Lapparent et al. (2003) and de Lapparent (2003). The LF parameters are extracted from Table 6 of de Lapparent et al. (2003) for the shape parameters (using Σ_2 for ellipticals and Centaurus parameters for dE+dS0 and Im+BCD galaxies) and from Table 1 of de Lapparent (2003) for the amplitudes ϕ^* . The mapping made between the LF morphological types and the EFIGI types is given in Table 2. Colour conversion terms between the Johnson-Cousins system and SDSS system are extracted from Jordi et al. (2006).

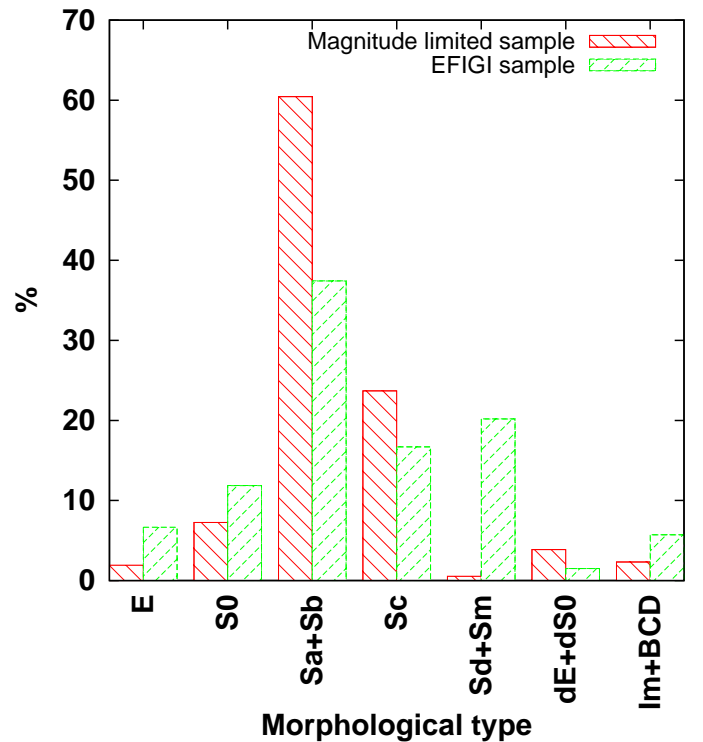


Fig. 29. Comparison between the observed EFIGI catalogue type mix (in green) and the expected type mix from a magnitude-limited sample with $g < 15.75$ (in red).

Table 2. Morphological type mapping between luminosity function types and EFIGI types.

LF types	EFIGI types
E	cE, E, cD
S0	S0 ⁻ , S0 ⁰ , S0 ⁺
Sa/Sb	S0/a, Sa, Sab, Sb, Sbc
Sc	Sc, Scd
Sd/Sm	Sd, Sdm, Sm
dE+dS0	dE
Im+BCD	Im

The galaxy counts per morphological type are then calculated as:

$$N_T = \int_{-\infty}^{-10} \phi_T(M) V_{lim}(M) dM; \quad (1)$$

$\phi_T(M)$ is the LF for Hubble type T and V_{lim} the volume defined as

$$V_{lim}(M) = \frac{\Omega}{3} 10^{0.6(g_{lim}-M)-15}, \quad (2)$$

where Ω is the solid angle (6670 deg²), and g_{lim} is the g -band apparent magnitude limit of the sample. Based on Fig. 25 above, and Fig. 3 of de Lapparent et al. (2011), we use $g_{lim} = 15.75$.

The differential fractions $\frac{dN_T}{dM}$ for the various galaxy types are plotted in Fig. 28, and the integrated fractions obtained from the homogenised EFIGI catalogue are shown in Fig. 29. The giant galaxy types (E) dominate at $M - 5 \log h \leq -22.5$ whereas small spirals (Sd+Sm), Im and dE contribute significantly at $M - 5 \log h > -18$. As a result, the difference in morphological fractions between the EFIGI catalogue and the LF predictions are for Sd+Sm galaxies which are largely missing in the (bright)

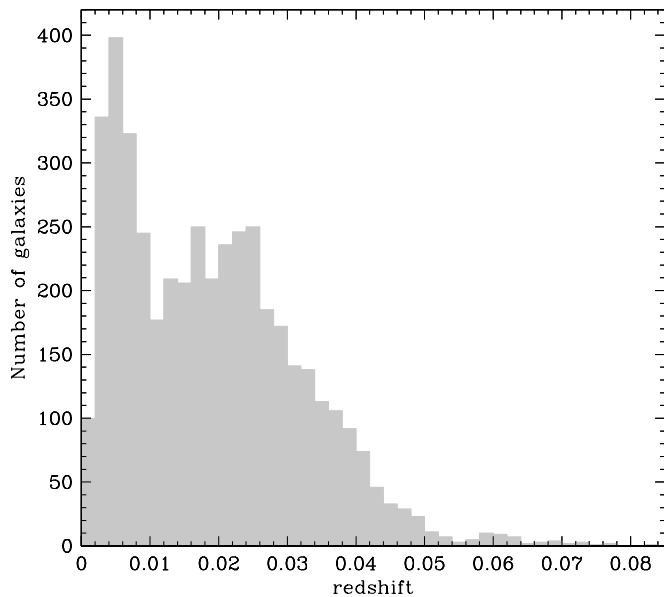


Fig. 30. The redshift distribution of the 4437 EFIGI galaxies with a redshift measurement. The peak at $z \approx 0.004$ is due to the Virgo Cluster.

magnitude-limited sample. The opposite occurs for Sa+Sb types. The EFIGI sample also recovers three times and twice more E and Im galaxies resp., whereas it undersamples the Sa+Sb and the Sc types by $\sim 30\%$ compared to the magnitude-limited sample.

5.6. Redshift distribution

The redshift completeness of the EFIGI catalogue is high: 4437 of the 4458 EFIGI galaxies have a redshift, that is 99.53%; $\sim 90\%$ of redshifts are from HyperLeda, $\sim 9\%$ from NED, the rest from SDSS (see de Lapparent et al. 2011 for details). The majority of galaxies in the catalogue (4365 over 4458) have $z < 0.05$ as shown on Fig. 30, which is consistent with the RC3 selection process ($cz < 15,000 \text{ km s}^{-1}$). This graph also shows that the redshift distribution of the EFIGI catalogue differs from that for a magnitude-limited sample by having a denser sampling at redshifts lower than the peak of the redshift distribution ($z \sim 0.025$). Moreover, the Virgo Cluster contains nearly half of the galaxies with $z \leq 0.01$.

Fig. 31 displays 3 pie-diagrams, 2 for the northern galactic cap, and one for the 3 strips in the southern galactic cap. Despite the spatially inhomogeneous sampling of the EFIGI catalogue, the large-scale structure of the universe is visible, with clusters, voids and walls (de Lapparent et al. 1986).

6. Comparison with Nair & Abraham (2010)

Nair & Abraham (2010, NA2010 hereafter) have recently released a morphological catalogue of 14 034 visually classified SDSS galaxies extracted from the SDSS DR4 spectroscopic release. The NA2010 catalogue is limited to objects brighter than SDSS g -band magnitude 16, and lie within a redshift interval $0.01 < z < 0.1$. In addition to a morphological type based on the RC3 classification, a number of flags describing the morphological appearance of bars, rings, lenses, and perturbation features are provided. Bar strength is divided in four levels: no bar, weak, intermediate, strong. Others feature indicators are strictly

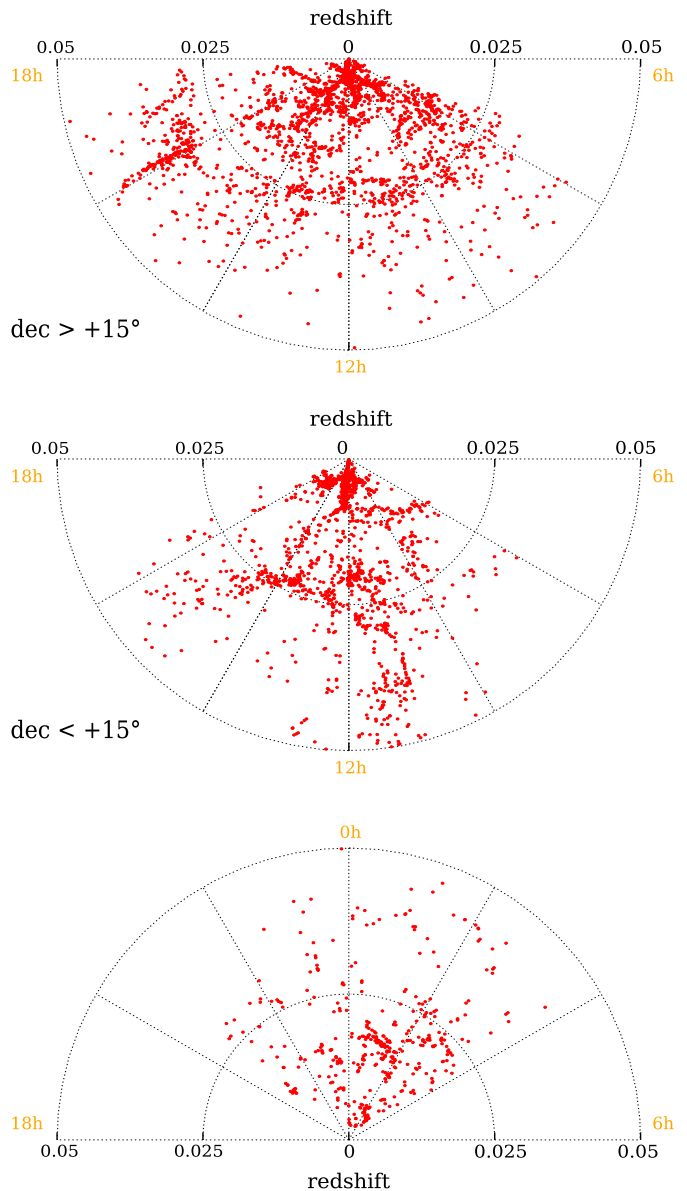


Fig. 31. Redshift pie-diagrams of EFIGI galaxies. The top panel corresponds to $6\text{h} < \alpha < 18\text{h}$ and $\delta > 15^\circ$. Middle panel: $6\text{h} < \alpha < 18\text{h}$ and $\delta < 15^\circ$. Bottom panel: $18\text{h} < \alpha < 6\text{h}$.

binary. The NA2010 galaxy type is based on g -band images only, whereas morphological flags rely also on r and i images when necessary, in order to confirm the presence of certain features.

Despite the significantly different classification criteria used by NA2010, a rough comparison with the EFIGI catalogue can be made for the morphological type and some features in common between both catalogues: perturbation, bar length, inner ring, outer ring, and pseudo-ring (Fig. 32). One third of EFIGI galaxies have redshifts below the $z = 0.01$ cut-off in NA2010, and 15% have SDSS (incorrect) g magnitudes > 16 , hence only 1438 galaxies are in common within a cross-identification radius of 20 arcsec, that is about 10% of the NA2010 sample.

A comparison of Hubble types between both catalogues (Fig. 32, top left) exhibits essentially the same systematic features as Fig. 14 of NA2010 (comparison with the RC3 catalogue). This is not surprising since the EFIGI classification scheme is very close to the RC3 system (Fig. 19). NA2010 do

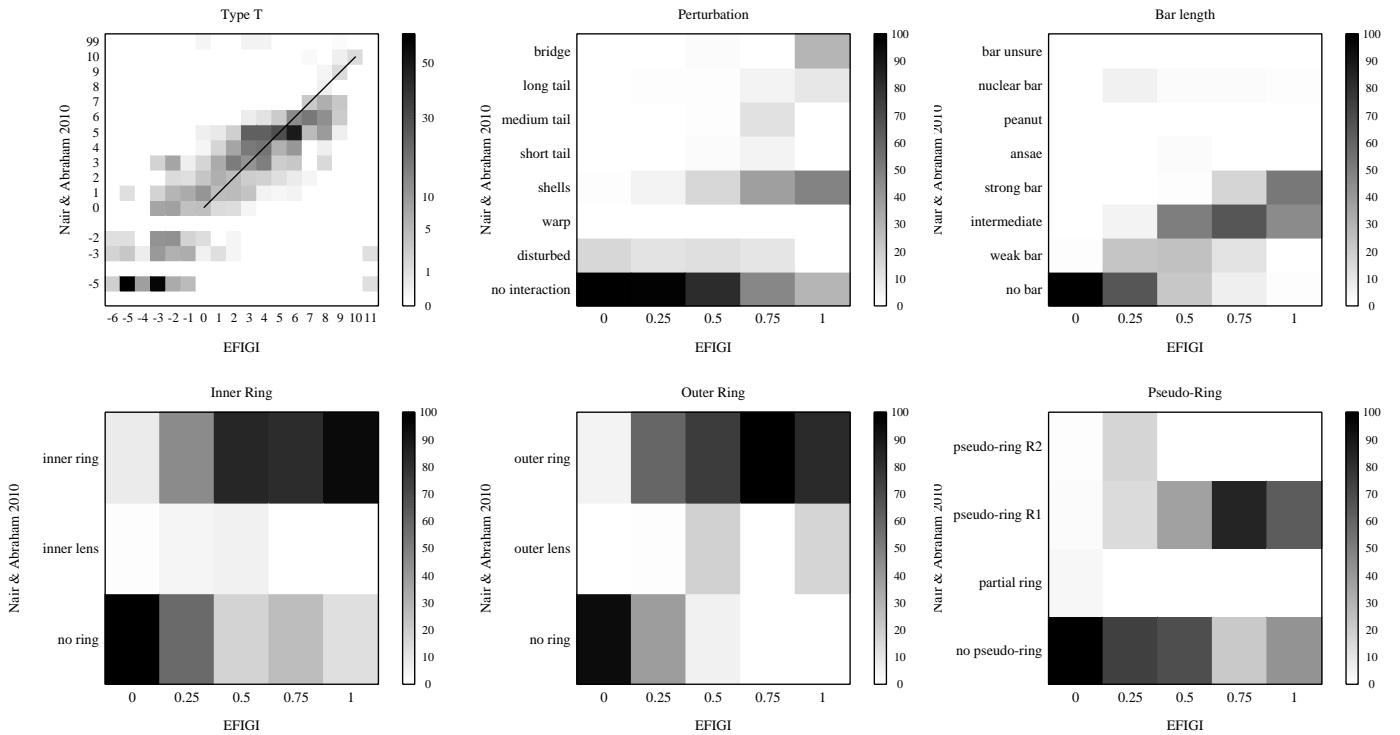


Fig. 32. Comparison between the EFIGI and the Nair & Abraham (2010) classifications for the 1438 galaxies in common with both catalogues. From left to right, top to down: EFIGI Hubble type (the straight line indicates perfect agreement), perturbation, bar length, inner ring, outer ring, and pseudo-ring attributes are compared to the Hubble type and corresponding features recorded by Nair & Abraham (2010). Results are shown in the form of confusion matrices; the contribution of each galaxy is weighted as in Fig. 21. For the Hubble type, cell values are proportional to the effective number of galaxies per cell (with the corresponding numbers indicated on the vertical scale on the right). For the attributes, cell values are expressed in percentage of the total effective number of galaxies per EFIGI attribute bin.

not distinguish between cE, cD, dwarf spheroidal and “regular” ellipticals. Galaxies classified as lenticulars or early spirals (Sa, Sab, Sb, Sbc) in the EFIGI catalogue are, in average, shifted towards later stages in NA2010. An opposite effect is seen for later spirals (Sc, Scd, Sd). The agreement for Sdm, Sm and Im seems better, although this only comes from a handful of galaxies; in total these types comprise $\sim 1\%$ of all NA2010 galaxies, compared to $\sim 20\%$ in the EFIGI sample.

Comparing the EFIGI perturbation index to NA2010 “distortion” flags sheds light on the staging process. First of all, a major fraction of galaxies described as slightly or moderately “perturbed” in the EFIGI catalogue are not flagged as distorted in NA2010, which we interpret as suggesting the EFIGI classification might be more sensitive towards relatively “benign” features such as spiral arm asymmetry. Although there is a clear trend towards galaxies with higher perturbation indices containing a higher fraction of tails, bridges or shells (up to $\sim 70\%$ altogether for galaxies with perturbation = 1), the fraction of objects classified as “disturbed” by NA2010 is essentially stable along the perturbation sequence, at about 10%.

The bar length EFIGI index appears to follow very closely the scale set by “bar strength” flags in NA2010. We note that bars with EFIGI bar length = 0.25 to 0.75 are detected in the EFIGI catalogue for a fraction of objects with “no bar” in NA2010, whereas there is essentially no case of bar detection in NA2010 for EFIGI objects with bar length = 0. Finally, galaxies flagged as having a nuclear bar in NA2010 are consistently assigned a bar length of 0.25 in the EFIGI sample.

There is also a good agreement between the NA2010 ring flags and the EFIGI inner ring and outer ring attributes.

The $\sim 30\%$ to $\sim 60\%$ of EFIGI galaxies with a value of 0.25 for inner ring and outer ring resp. maybe be due to tight spiral arms in a galaxy centre resembling a ring for the former attribute, and to portions of rings for the latter; the former may not have activated the NA2010 inner ring flag, whereas the latter may have activated instead the NA2010 “distortion” flag for tails or shells. The inner and outer lenses were deliberately graded as inner ring and outer ring resp. in the EFIGI sample. Comparison with the NA2010 “inner lens” and “outer lens” flags indicates that lenses in EFIGI galaxies amount to up to 6% for inner ring and up to 18% for outer ring.

The comparison of the EFIGI pseudo-ring attribute with the corresponding NA2010 flags confirms the inclusion of both R'_1 and R'_2 types into this EFIGI attribute, with respective attribute values of 0.75-1.0 and 0.25-0.5 (see Sect. 3.2). The additional EFIGI detections with pseudo-ring attribute values of 0.25-0.5 whereas the flag is not activated in NA2010 are likely to correspond to $R'_1R'_2$ types, which are not flagged in NA2010. There is also a number of EFIGI galaxies with R'_1 rings (pseudo-ring attribute values of 0.75-1.0) which have not been flagged by NA2010.

To conclude, EFIGI perturbation, bar and ring attributes are in good agreement with the corresponding NA2010 flags. It is unclear whether the low level detections in EFIGI testify to higher sensitivity or false detections; in principle the combination of a five-level scale and a confidence interval for every EFIGI attribute is expected to provide the best representation of marginally detectable features.

7. Summary and perspectives

We present the EFIGI catalogue, a multiwavelength catalogue of 4458 galaxies selected from the PGC and observed with the SDSS. The catalogue provides detailed morphological information using 16 morphological attributes: B/T ratio, arm strength, arm curvature, rotation, visible dust, dust dispersion, flocculence, hot spots, bar length, inner ring, outer ring, pseudo-ring, perturbation, inclination/elongation, multiplicity, contamination. These attributes are defined on a five-level scale, and describe the internal properties and the different components of a galaxy: bulge, spiral arms, dynamical features, textural aspect, as well as its appearance and environment. All galaxies are also classified along a morphological sequence based on the RC3 Revised Hubble Sequence.

The EFIGI catalogue (attributes and Hubble type), complemented by identification, morphological and redshift data from the PGC, SDSS, HyperLeda and NED, is available on the <http://www.efigi.org> website, along with additional imaging products: FITS image data, colour images, and PSF models. The catalogue is also available from the “Centre de Données Astronomiques de Strasbourg” (CDS) using the ViZiER Catalogue Service. Here we show, for the 5 levels of each attribute, composite colour images of representative and atypical galaxies over a wide variety of Hubble types.

Various statistical tests demonstrate the reliability of this morphological description. We find a remarkable level of agreement between the RC3 Revised Hubble Sequence and the EFIGI Hubble sequence over the 15 common classes, despite classifications being carried out by different astronomers based on different imaging material. Moreover, the sky distribution of the weighted average attribute strengths shows for all 16 attributes the absence of obvious trends as a function of right ascension along which EFIGI galaxies are ordered. The projected sky distribution of the EFIGI catalogue also shows that it covers the whole area of the SDSS Data Release 4, with ten known clusters of galaxies identified as concentrations of more than 5 galaxies in the catalogue.

Confusion matrices of the 16 attributes quantify the strong correlation observed between the B/T ratio and arm curvature, a major criterion for defining the progression of spiral types along the Hubble sequence. The anti-correlations between the B/T ratio and the various other attributes that increase in strength along the Hubble sequence, flocculence, hot spots, perturbation, and arm strength, are also highlighted. These latter attributes, together with visible dust are correlated among themselves because they are related indicators of the star formation in a galaxy. The perturbation attribute is also strongly correlated with both hot spots and flocculence, as tidal and merging processes contribute to enhance star formation. We also detect the strong correlation between internal ring and bar length.

Contrary to the bell-shape B_T magnitude distribution, the SDSS $ugriz$ distributions show faint extensions (for Petrosian magnitudes fainter than ~ 20 in u and fainter than ~ 17 in g , r , i , and z). This reflects the failure of the SDSS photometric pipeline for large late-type spirals and irregular galaxies which are split into multiple units. More details are provided in de Lapparent & Bertin (2011a, in prep.) where unbiased photometric properties are derived for all EFIGI galaxies using a new version of SExtractor (Bertin & Arnouts 1996) incorporating model-fitting capabilities (Bertin 2011).

We show that the EFIGI catalogue is a dense sub-sample of the local Universe: over the area of the SDSS DR4, its photometric completenesses at bright magnitudes (14.5 in u and 12.5 – 13.5 in g , r , i , and z) are $\sim 80\%$ in the u and g filters, and $\sim 85\%$ in the r , i , z filters. This is much higher than the raw completenesses calculated from the SDSS photometry: $\sim 30\%$ in u and $\sim 60 - 70\%$ in g , r , i , and z . When examining the SDSS galaxies not present in the EFIGI catalogue at bright magnitudes, we found that 90% of the sources are spurious and are caused by haloes of a bright saturated stars, or less frequently, by satellite trails.

Most of EFIGI galaxies (99.53%) have a redshift (mostly from the HyperLeda database), and the vast majority have $z \lesssim 0.05$. Pie-diagram redshift maps show the large-scale clustering of galaxies, with a strong contribution from the Virgo cluster at $z \lesssim 0.01$.

Comparison of the EFIGI morphological type fractions with the typical expectations for a magnitude-limited sample of the local Universe show that the EFIGI catalogue largely oversamples late-type spirals (Sd, Sdm, Sm) and irregulars. These types are as or more numerous than the EFIGI early types (E, S0⁻, S0, S0⁺, Sa, Sab). The late types also appear mainly at redshift $z \lesssim 0.03$, due to their faint absolute magnitude, whereas earlier types are present at all redshifts. As shown by de Lapparent et al. (2011), this is a consequence of the apparent diameter limit of the EFIGI catalogue.

As a first application, the EFIGI morphological attributes were used for supervised learning tasks: using “Support Vector Machines” Baillard (2008) showed that one can determine the Hubble type from a reduced number of EFIGI attributes, which are, in decreasing order of significance: the bulge-to-total luminosity ratio, the strength of spiral arms, the curvature of spiral arms; the amount of visible dust and flocculence play a less significant role in determining the Hubble type.

An experimental test of the automatic determination of morphological attributes has also been performed within SExtractor, using a projection of the residual profiles onto ring-based functions (Baillard 2008). More recently, Perret et al. (2011) have applied an MCMC algorithm with multiple temperature simulated annealing to the EFIGI image data-set to perform multispectral decompositions of galaxy components. Ultimately, merging an automatic determination of the morphological estimators with the determination of the Hubble Type should allow one to perform a fully automatic determination of the Hubble Type from galaxy images.

The dense sampling of all Hubble types by the EFIGI catalogue, and its high photometric and spectroscopic completenesses make this catalogue directly usable for statistical analyses of the galaxy distribution at low redshift. A companion article (de Lapparent et al. 2011) reports on the statistical analysis of the EFIGI morphological attributes, and provides for the first time a quantitative description of the Hubble Sequence in terms of specific morphological features.

Two other articles further use the EFIGI catalogue to study the properties of nearby galaxies: the bulge and disk properties along the Hubble sequence (de Lapparent & Bertin, 2011a, in prep.), using the new profile fitting tools within SExtractor (Bertin & Arnouts 1996; Bertin 2011); the luminosity functions as a function of morphological type and galaxy component (de Lapparent & Bertin, 2011b, in prep.). The first of these analyses illustrates the usefulness of a well-defined calibration sample for application of the automatic tools for measuring galaxy morphometry. Detailed analyses at low redshift are also indispensable for understanding the evolution of galaxy morphome-

try with look-back time using deeper imaging as in the Canada-France-Hawaii Telescope Legacy survey.

Acknowledgements. We are grateful to the referee, Ron Buta, for his very useful comments. This work has been supported by grant 04-5500 (“ACI masse de données”) from the French Ministry of Research.

This research made use of the HyperLeda database (<http://leda.univ-lyon1.fr>), the VizieR catalogue access tool (Ochsenbein et al. 2000) and the Sesame service at CDS (Strasbourg, France), and the NASA/IPAC Extragalactic Database (NED), which is operated by the Jet Propulsion Laboratory, California Institute of Technology, under contract with the National Aeronautics and Space Administration.

This publication also made use of the Sloan Digital Sky Survey. Funding for the SDSS and SDSS-II has been provided by the Alfred P. Sloan Foundation, the Participating Institutions, the National Science Foundation, the U.S. Department of Energy, the National Aeronautics and Space Administration, the Japanese Monbukagakusho, the Max Planck Society, and the Higher Education Funding Council for England. The SDSS Web Site is <http://www.sdss.org/>. The SDSS is managed by the Astrophysical Research Consortium for the Participating Institutions. The Participating Institutions are the American Museum of Natural History, Astrophysical Institute Potsdam, University of Basel, University of Cambridge, Case Western Reserve University, University of Chicago, Drexel University, Fermilab, the Institute for Advanced Study, the Japan Participation Group, Johns Hopkins University, the Joint Institute for Nuclear Astrophysics, the Kavli Institute for Particle Astrophysics and Cosmology, the Korean Scientist Group, the Chinese Academy of Sciences (LAMOST), Los Alamos National Laboratory, the Max-Planck-Institute for Astronomy (MPIA), the Max-Planck-Institute for Astrophysics (MPA), New Mexico State University, Ohio State University, University of Pittsburgh, University of Portsmouth, Princeton University, the United States Naval Observatory, and the University of Washington.

References

- Abraham, R., van den Bergh, S., & Nair, P. 2003, *ApJ*, 588, 218
- Adelman-McCarthy, J. K., Agüeros, M. A., Allam, S. S., et al. 2006, *ApJS*, 162, 38
- Baillard, A. 2008, Ph.D. Thesis
- Bertin, E. 2011, in *Astronomical Data Analysis Software and Systems XX*, in press
- Bertin, E. & Arnouts, S. 1996, *Astronomy and Astrophysics, Suppl. Ser.*, 117, 393
- Bertin, E., Delorme, P., Baillard, A., Marmo, C., & Semah, G. 2011, in preparation
- Bertin, E., Mellier, Y., Radovich, M., et al. 2002, 281, 228
- Bertin, G. & Lin, C. 1996, *Spiral Structure in Galaxies* (The MIT press)
- Binggeli, B. & Cameron, L. M. 1991, *A&A*, 252, 27
- Blanton, M. R. & Roweis, S. 2007, *AJ*, 133, 734
- Blanton, M. R., Schlegel, D. J., Strauss, M. A., et al. 2005, *AJ*, 129, 2562
- Block, D. L., Puerari, I., Knapen, J. H., et al. 2001, *A&A*, 375, 761
- Bonnarel, F., Fernique, P., Bienaymé, O., et al. 2000, *A&AS*, 143, 33
- Buta, R. & Combes, F. 1996, *Fund. Cosmic Phys.*, 17, 95
- Buta, R., Laurikainen, E., Salo, H., Block, D. L., & Knapen, J. H. 2006, *AJ*, 132, 1859
- Buta, R. J. 2011, *ArXiv e-prints*
- Colpi, M., Gorini, V., Haardt, F., & Moschella, U. 2006, *Joint Evolution of Black Holes and Galaxies* (Taylor and Francis Group)
- de Jong, R., Simard, L., Davies, R., et al. 2005
- de Lapparent, V. 2003, *A&A*, 408, 845
- de Lapparent, V., Baillard, A., & Bertin, E. 2011, *A&A*, in press
- de Lapparent, V. & Bertin, E. 2011a, in preparation
- de Lapparent, V. & Bertin, E. 2011b, in preparation
- de Lapparent, V., Galaz, G., Bardelli, S., & Arnouts, S. 2003, *A&A*, 404, 831
- de Lapparent, V., Geller, M. J., & Huchra, J. P. 1986, *ApJ*, 302, L1
- de Vaucouleurs, G. 1959, *Handbuch der Physik*, 53, 275
- de Vaucouleurs, G., de Vaucouleurs, A., Corwin, Jr., H. G., et al. 1991, *Third Reference Catalogue of Bright Galaxies* (Volume 1-3, XII, 2069 pp. 7 figs.. Springer-Verlag Berlin Heidelberg New York)
- de Vaucouleurs, G., de Vaucouleurs, A., & Corwin, J. R. 1976, in *Second reference catalogue of bright galaxies*, 1976, Austin: University of Texas Press., 0–+
- Dressler, A. 1980, 236, 351
- Dunkley, J., Komatsu, E., Nolta, M. R., et al. 2009, *ApJS*, 180, 306
- Ferguson, H. C. & Binggeli, B. 1994, *A&A Rev.*, 6, 67
- Freedman, W. L., Madore, B. F., Gibson, B. K., et al. 2001, *ApJ*, 553, 47
- Gray, M. E., Wolf, C., Barden, M., et al. 2009, *MNRAS*, 393, 1275
- Hubble, E. P. 1936, *Realm of the Nebulae*, ed. Hubble, E. P.
- Hunt, L. & Malkan, M. 1999, *ApJ*, 516, 660
- Jordi, K., Grebel, E. K., & Ammon, K. 2006, *A&A*, 460, 339
- Kormendy, J. 1979, *ApJ*, 227, 714
- Kormendy, J., Fisher, D. B., Cornell, M. E., & Bender, R. 2009a, *ApJS*, 182, 216
- Kormendy, J., Fisher, D. B., Cornell, M. E., & Bender, R. 2009b, *ApJS*, 182, 216
- Laurikainen, E., Salo, H., & Rautiainen, P. 2002, *MNRAS*, 331, 880
- Lintott, C. J., Schawinski, K., Slosar, A., et al. 2008, *MNRAS*, 389, 1179
- Naim, A., Ratnatunga, K. U., & Griffiths, R. E. 1996
- Nair, P. B. & Abraham, R. G. 2010, *ApJS*, 186, 427
- Ochsenbein, F., Bauer, P., & Marcout, J. 2000, *A&AS*, 143, 23
- Paturel, G., Fouque, P., Bottinelli, L., & Gouguenheim, L. 1995, *VizieR Online Data Catalog*, 7119, 0
- Paturel, G., Petit, C., Prugniel, P., et al. 2003, *A&A*, 412, 45
- Perret, B., Mazet, V., Collet, C., & Slezak, E. 2011, *Pattern Recognition*, in press
- Postman, M. & Geller, M. J. 1984, *ApJ*, 281, 95
- Roberts, M. & Haynes, M. 1994, *ARA&A*, 32, 115
- Sandage, A. & Binggeli, B. 1984, 89, 919
- Schaaff, A. 2004, 314, 327
- Seigar, M., Kennefick, D., Kennefick, J., & Lacy, C. 2008, *ApJ*, 678, L93
- van den Bergh, S. 1998, *Galaxy Morphology and Classification*, ed. van den Bergh, S.

Appendix A: Data products and tables

The EFIGI catalogue is available at CDS and in the dedicated website <http://www.efigi.org>. The catalogue contains for each object the EFIGI morphological type and 16 morphological attributes as listed in Table A.1; although not indicated in Table A.1 for clarity reasons, we provide for each attribute the lower and upper bound of its confidence interval. We also provide the centred coordinates (see Sect. 2.2), the selected heliocentric and Virgo-infall corrected redshifts and comoving, luminosity and angular diameter distances, as listed in Table A.2. We convert redshifts into distances using a Hubble constant $H_0 = 70$ km/s/Mpc (Freedman et al. 2001), and the currently standard cosmological parameters $\Omega_m = 0.3$ and $\Omega_\Lambda = 0.7$ (Dunkley et al. 2009).

We then provide the various PGC parameters listed in Table A.3, the HyperLeda parameters listed in Table A.4, the NED parameters listed in Table A.5, and the SDSS parameters listed in Table A.6. Additional HyperLeda and NED parameters can be retrieved from these tables using the listed PGC identifiers, and additional SDSS parameters can be retrieved using the listed SDSS identifiers.

For each EFIGI galaxy, we also provide in the <http://www.efigi.org> website: *ugriz* FITS images, a composited *irg* “true colour” image in PNG format (see Sect. 2.2), and the *ugriz* PSF models (see Sect. 4).

Table A.1. EFIGI attributes

PGC_name	PGC name
T	EFIGI morphological type
Bulge_to_Total	Bulge-to-total ratio
Arm_Strength	Strength of spiral arms
Arm_Curvature	Average curvature of the spiral arms
Arm_Rotation	Winding direction of the spiral arms
Bar_Length	Length of central bar
Inner_Ring	Strength of inner ring, lens or pseudo-ring
Outer_Ring	Strength of outer ring
Pseudo_Ring	Type and strength of outer pseudo-ring
Perturbation	Deviation from a profile with rotational symmetry
Visible_Dust	Strength of dust features
Dust_Dispersion	Patchiness of dust features
Flocculence	Strength of scattered HII regions
Hot_Spots	Strength of regions of strong star formation, active nuclei, or stellar nuclei
Inclination	Inclination of disks or elongation of spheroids
Contamination	Severity of contamination by stars, galaxies or artifacts
Multiplicity	Abundance of neighbouring galaxies

Table A.2. EFIGI fields

PGC_name	PGC name
RA	Right ascension J2000 (degrees)
DEC	Declination J2000 (degrees)
z_hel	Selected heliocentric redshift
z_hel_err	Uncertainty in selected heliocentric redshift
z_dis	Selected redshift corrected for Local Group infall into Virgo
z_dis_err	Uncertainty in selected redshift corrected for Local Group infall into Virgo
D_com	Comoving distance derived from z_dis or z_hel (Mpc)
D_lum	Luminosity distance derived from z_dis or z_hel (Mpc)
D_diam	Transverse diameter distance derived from z_dis or z_hel (Mpc)

Table A.3. PGC fields

PGC_name	PGC name
T_PGC	RC3 morphological type
e_T_PGC	Mean error on T_PGC
type	Expanded morphological type
D25	$\log D_{25}$, decimal logarithm of mean apparent major isophotal diameter measured at or reduced to surface brightness level $\mu_B = 25.0 \text{ mag.arcsec}^{-2}$ (in units of 0.1 arcmin)
R25	$\log R_{25}$, decimal logarithm of ratio of mean major isophotal diameter, D_{25} , to mean minor isophotal diameter measured at or reduced to the surface brightness level $\mu_B = 25.0 \text{ mag.arcsec}^{-2}$
PA	Position angle of major axis (degrees)
B_T_mag	Total B magnitude
e_B_T_mag	Mean error on B_T_mag
B_V_T	Total (B-V)
e_B_V_T	Mean error on total (B-V)
cz	Heliocentric velocity (km/s)
z	Redshift

Table A.4. HyperLeda fields

PGC_name	PGC name
PGC_no	PGC number
vrad	Heliocentric radial velocity from radio measurement (km/s)
e_vrad	Actual error on vrad (km/s)
vopt	Heliocentric radial velocity from optical measurement (km/s)
e_vopt	Actual error on vopt (km/s)
v	Mean heliocentric radial velocity (km/s)
e_v	Actual error on v (km/s)
vvir	Radial velocity corrected for Local Group infall into Virgo (km/s)
zvir	Redshift corrected for Local Group infall into Virgo
z_err	Redshift error derived from e_v
type	Morphological type
objname	Principal designation
hl_names	List of all object names

Table A.5. NED fields

PGC_name	PGC name
cz	Heliocentric velocity (km/s)
redshift	Redshift
nedname	Object name

Table A.6. SDSS fields

PGC_name	PGC name
objID	Unique SDSS photometric identifier composed from skyVersion, rerun, run, camcol, field, obj
specObjID	Unique SDSS spectroscopic identifier
z	Redshift
zErr	Uncertainty in redshift
zConf	Confidence level in redshift